De novo deletion mutations at recombination hotspots in mouse germlines

Agnieszka Lukaszewicz[1], Julian Lange[2], Scott Keeney[2,3], Maria Jasin[1]

[1]Developmental Biology Program, [2]Molecular Biology Program, and [3]Howard Hughes Medical Institute, Memorial Sloan Kettering Cancer Center, New York, NY, USA

To whom correspondence should be addressed:
Scott Keeney: s-keeney@ski.mskcc.org
Maria Jasin: m-jasin@ski.mskcc.org, Lead contact

Abstract

Numerous DNA double-strand breaks (DSBs) arise genome-wide during meiosis to ensure recombination between homologous chromosomes, which is required for gamete formation[1,2]. The ATM kinase plays a central role in controlling both the number and position of DSBs[3-5], but the consequences of deregulated DSB formation have not been explored. Here we discovered that an unanticipated type of DNA deletion arises at meiotic recombination hotspots in the absence of ATM. Deletions form via joining of ends from two closely-spaced DSBs at adjacent hotspots or within a single hotspot. Deletions are also detected in normal cells, albeit at much lower frequency, revealing that the meiotic genome has a hidden potential for deletion events. Remarkably, a subset of deletions contain insertions that likely originated from DNA fragments released from hotspots on other chromosomes. Moreover, although deletions form primarily within one chromosome, joining between homologous chromosomes is also observed. This predicts in turn gross chromosome rearrangements, with evidence of damage to multiple chromatids and aborted gap repair. Thus, multiple nearby meiotic DSBs are normally suppressed by ATM to protect genomic integrity. We expect the *de novo* germline mutations we observe to affect human health and genome evolution.

Meiotic recombination is essential for faithful genome transmission in most sexually reproducing organisms[2]. Recombination is initiated by the programmed formation of DNA double-strand breaks (DSBs) by the SPO11 protein[6]. SPO11 preferentially cuts within narrow genomic regions called hotspots[7,8], usage of which is tightly regulated. Of all DSB hotspots (~15,000 defined in mouse), only a tiny fraction (~250) experiences a DSB in any single meiosis[9-11]. DSBs are also nonrandomly dispersed along chromosomes to ensure homolog pairing and recombination[3]. This quantitative and spatial regulation of hotspot usage involves hierarchical and combinatorial levels of control[9,12,13], with the ATM kinase playing a central role[5,14].

ATM, known for its role in the DNA damage response in mitotic cells[15], is activated by meiotic DSBs to limit DSB numbers and to control hotspot usage genome-wide[4,9]. Control of DSB numbers by ATM and its orthologs is conserved among organisms, although ATM-deficient mice have the largest increase in DSB levels (e.g., ~10 fold compared with ~2 fold in budding yeast deficient for the ATM ortholog Tel1)[5,16,17]. Control of genome-wide DSB distributions is also conserved[18]. In yeast, Tel1 controls DSB formation locally by suppressing double cutting, that is, simultaneous DSB formation at adjacent hotspots[14,19]. This suppression is strongest at closely-spaced hotspots (<10 kb), such that in the absence of Tel1, double cutting at hotspots separated by ~2 kb is more frequent than expected by chance and ~10-fold higher than in wild type. The loss of this Tel1-mediated DSB suppression is thought to contribute to the global increase in DSBs[18,19]. In mouse, double cutting at adjacent hotspots has not been demonstrated, but potentially may be even more likely in the absence of ATM, considering the extremely elevated DSB numbers. Accordingly, we have previously suggested that ATM may inhibit multiple nearby DSBs[4,9].

The consequences of deregulated meiotic DSB formation on genomic architecture are not fully understood. Normally, most meiotic DSBs are repaired by recombination between homologous chromosomes to promote their segregation in meiosis I. We speculate that in the absence of ATM, too many DSBs and closely-spaced DSBs interfere with the meiotic recombination program, eliciting the use of other repair pathways, in particular, mutagenic nonhomologous end-joining (NHEJ), and thus compromising genome integrity. While NHEJ is a robust mitotic DSB repair pathway in mice[20], it is thought to normally be suppressed in meiosis[21]. However, NHEJ can occur in mouse spermatocytes when DSBs are induced by irradiation[22-24], and it is known to operate in *C. elegans* in meiotic mutants in which DSB processing[25-27] or recombination[28,29] is compromised. In principle, because ATM/Tel1 regulates meiotic DSB resection[30-34], resection defects could favor the use of NHEJ. Moreover, the loss of ATM may cause DSBs to form at similar locations on multiple chromatids – due to the increase in DSB numbers and/or the loss of spatial control – and thus promote NHEJ by damaging repair templates.

In this report, we ask whether multiple DSBs form at adjacent hotspots in the absence of ATM in mouse spermatocytes and whether they are repaired aberrantly to delete the intervening sequences. Further, we ask whether multiple DSBs leading to deletions can occur within an individual hotspot. In the course of these experiments, we uncover novel DSB (mis)repair products that provide insight into the consequences of loss of DSB control during meiosis.

Results

Hidden potential of the meiotic genome to form deletions

We first catalogued genomic locations at risk for deletion by identifying pairs of closely-spaced hotspots in nucleotide-resolution DSB maps obtained by sequencing SPO11-bound oligonucleotides (oligos), a by-product of DSB formation[9]. We found that numerous DSB hotspots are separated by a short genomic distance (**Fig. 1A**). For example, ~6% of 13,436 autosomal SPO11-oligo hotspots in wild-type mice are located within 5 kb of another hotspot, and this percentage nearly doubles (~10%) in *Atm*$^{-/-}$ mice, which have more called hotspots (20,417) (**Fig. S1A**). Most hotspots in *Atm*$^{-/-}$ mice are shared with those in wild type, although a significant fraction are newly called because the few SPO11 oligos that cluster at these sites in wild type are greatly increased in the mutant[9] (**Fig. S1A**). Newly called hotspots often emerge near shared hotspots, resulting in an increased number of closely-spaced hotspots in *Atm*$^{-/-}$ (**Fig. S1B**). Moreover, in addition to the number, the strength of the shared hotspot pairs also disproportionately increases in *Atm*$^{-/-}$ (**Fig. S1C**), at least in part due to the particularly large increase in DSBs at weaker hotspots[9]. Thus, while adjacent DSBs may normally be suppressed, this hidden potential for DSBs at adjacent hotspots may be revealed in *Atm*$^{-/-}$.

To test for deletions, we selected DSB hotspot pairs that are shared between wild type and mutant and that contain strong hotspots to increase the chance of simultaneous DSB formation. The chosen hotspot pairs on Chr1 and Chr19 are separated by <2 kb, with individual hotspots that rank in the top quartile of all hotspots in both wild type and *Atm*$^{-/-}$ (**Fig. 1B, S1D, S2A**). We tested for deletions between the two hotspots in each pair by performing nested PCR on testis DNA. Concurrent DSB formation at the hotspot centers with precise joining of the DNA ends would give rise to 1.8-kb deletions, although deletions could vary in size depending on the location of SPO11 cleavage in any particular cell (**Fig. 1B, S2A**). Genomic DNA was digested with restriction enzymes prior to amplification in some experiments to suppress amplification of parental DNA. Nested PCR was performed with input testis DNA equivalent to ~8,000–16,000 haploid genomes per well for a total of ~10–15 million haploid genomes per genotype (**Table S1**).

Smaller PCR products indicative of deletions between the two DSB hotspots were observed in *Atm*$^{-/-}$ (**Fig. 1C, S2B**). In adult *Atm*$^{-/-}$ mice, the frequencies of deletions at the Chr1 and Chr19 hotspot pairs were 9.14×10^{-6} and 4.25×10^{-6}, respectively, per haploid genome (**Fig. 1D; Table S1**). Deletions were also detected in ATM-proficient cells but were rare. At the Chr19 hotspot pair, the frequencies were 0.15×10^{-6} and 0.31×10^{-6} in wild type and *Atm*$^{+/-}$, respectively, reflecting a total of just six events, while no deletions were observed in *Spo11*$^{-/-}$. For the Chr1 hotspot pair, only two deletions were observed in ATM-proficient cells, although one was also observed in *Spo11*$^{-/-}$.

Similar results were obtained in juvenile testes at both hotspot pairs at 15 days post partum, when wild-type and mutant testes have a similar distribution of prophase I stages. This finding indicates that the increase in deletion frequency is not due to the different cellular composition of mutant testes caused by prophase I arrest of *Atm*$^{-/-}$ spermatocytes[35,36] (**Table S1**).

It should be noted that testis DNA is derived from germ cells at different stages of development as well as from some somatic cells, such that the germline deletion frequencies we report are underestimated for all genotypes. Even so, meiotic recombination at a well-studied hotspot that has a similar strength as the individual hotspots examined here occurs at a substantially higher frequency (two to three orders of magnitude[37]) than the deletion frequency we observed at the hotspot pairs in the absence of ATM. However, considering the large number of hotspots located close to one another, the potential to form deletions in meiosis is substantial.

Double cutting in the absence of ATM

To map deletion breakpoints, we sequenced deletion products from *Atm*$^{-/-}$ adults and juveniles: 134 from the Chr1 hotspot pair and 58 from the Chr19 hotspot pair (**Fig. 2A, S2C; Table S2**). The distribution of deletion breakpoints resembled the distribution of SPO11 oligos at both hotspots, with breakpoints clustered around hotspot centers (**Fig. 2B,C, S2D,E**). Smoothed breakpoint and SPO11-oligo profiles displayed similar shapes, except that breakpoint profiles were slightly wider with more prominent smaller peaks (**Fig. 2D, S2F**). We defined the breakpoint center within each hotspot as the position of the smoothed peak in the breakpoint density, in the same manner as hotspot centers were defined[9]. Breakpoint centers closely matched both hotspot centers (within 13 to 42 bp). These findings strongly indicate that deletion formation is preceded by concurrent SPO11 cleavage at the two hotspots, providing the first evidence for double cutting between nearby DSB hotspots in mouse.

The median deletion lengths were similar to the distances between the DSB hotspot centers (Chr1: 1954 bp vs 1825 bp; Chr19: 1892 bp vs 1763 bp), as expected from SPO11 cleavage of both hotspots and joining of unprocessed or minimally processed DNA ends. Accordingly, a substantial number of deletions (Chr1, 21%; Chr19, 19%) had both breakpoints within the narrow (251 bp) central zones around the hotspot centers that contained the majority (>60%) of SPO11 oligos (**Fig. S3**). The distribution of events was similar when the restriction digest step was omitted (**Fig. S4**), indicating that this step does not eliminate other types of deletions. About half of the other deletions had one breakpoint within the central zone of one hotspot but not the other (Chr1, 41%; Chr19, 45%) (**Fig. S3**). Breakpoints outside the zone were not evenly distributed, such that some clusters could be observed that overlapped with, but were more prominent than, the SPO11-oligo distributions (**Fig. 2B–D, S2D–F**). While the similar distributions of breakpoints and DSBs suggests that DSB ends are usually joined close to the initial SPO11 cleavage sites, the wider distribution of deletion breakpoints may reflect preferential deletion formation for DSBs further from the hotspot center, DNA end processing prior to joining, or even multiple DSBs within the same hotspot (see below).

The few deletions identified in wild type and *Atm*$^{+/-}$ often had breakpoints at or near the hotspot centers, including some that were identical to those observed in *Atm*$^{-/-}$ (**Fig. S5**), consistent with their being *bona fide* deletions arising from concurrent DSBs. The one deletion obtained from *Spo11*$^{-/-}$ was between the two hotspots, with both breakpoints distant from the hotspot centers, which was observed only once in *Atm*$^{-/-}$.

Deletions occur primarily within one chromosome but can join homologous chromosomes

The deletions we observe predict double cutting at hotspot pairs within a single chromosome, however, in principle they could also arise from staggered DSBs on homologous chromosomes. To investigate whether deletions involve one or both homologs, we tested the Chr1 hotspot pair in B6 × DBA/2J (DBA) F1 hybrid males, which have a high polymorphism density across this region (**Fig. 3A**). Primers were shifted to amplify a larger fragment to aid in identifying the parental chromosome(s) involved in the deletion.

We recovered 37 deletions from *Atm*$^{-/-}$ testis DNA for a frequency of 4.20×10^{-6} per haploid genome, but none in the presence of ATM ($<0.16 \times 10^{-6}$) (**Table S1**). The distributions of deletion sizes (median 2046 bp) and breakpoints were broadly similar to those from B6 inbred mice (**Fig. 3A; S6A**). When we analyzed polymorphisms, 30 of the 34 informative deletions (88%) appeared to have originated within one chromosome: 10 on B6 and 20 on DBA (**Fig. 3A**). The higher frequency of deletions on the DBA chromosome might be associated with a polymorphism in the PRDM9 site at the left hotspot (**Fig. 3A,B**), which could positively affect DSB formation. The preponderance of deletions

181 within one chromosome indicates double cutting on a single chromosome (same chromatid or sister
182 chromatids), and supports a role for ATM in suppressing closely-spaced DSBs, like Tel1 in yeast[19].
183 Strikingly, however, we also captured four deletions that contained sequences from both
184 homologs (**Fig. 3A**). In one, the left hotspot from DBA was joined to the right hotspot from B6 (DBA-
185 Δ-B6). In the other three more complex events, a haplotype switch occurred adjacent to one of the
186 deletion breakpoints (DBA-B6-Δ-B6; DBA-B6-Δ-DBA, and B6-DBA-Δ-?, where the question mark
187 indicates that the genotype was uninformative at the right end). In these haplotype switches, 6–8
188 polymorphisms were incorporated, encompassing up to 500 bp (**Fig. 3A**).
189 The recovery of deletions involving interhomolog interactions shows that DSBs can occur at
190 nearby locations on both homologs in the same cell, at least in the absence of ATM, and, moreover,
191 that the DSB ends generated on the two homologs are capable of joining. Thus, although homolog
192 synapsis is greatly impaired in the absence of ATM[35,36], homolog interactions still occur. Cutting of
193 both homologs at the same hotspot has been inferred from patterns of strand exchange in yeast
194 tetrads[38-40].
195 Further, the three complex interhomolog events suggest that three or more DSBs had occurred
196 on the two homologs. One possible mechanism for the haplotype switch at a deletion breakpoint is
197 offset DSB formation on both homologs within the same hotspot, with attempted gap repair that is
198 aborted by the DSB in the template, followed by joining to a DSB at the other hotspot (**Fig. S6B**).
199 Alternatively, double cutting within one hotspot on one homolog might release a DNA fragment that
200 then inserts at the DSB in the other homolog (**Fig. S6C**). Irrespective of the precise mechanism,
201 however, these results indicate that loss of ATM can cause profound damage to multiple chromatids,
202 leading to deleterious types of repair.
203
204 **Sites of recurrent deletion breakpoints in the absence of ATM**
205
206 Most deletions between hotspots from *Atm*$^{-/-}$ mice were unique: 87% (161/185) of events on Chr1
207 were observed only once, as were 97% (56/58) for Chr19 (**Table S2**). Microhomologies were present
208 at the breakpoints in 70% of all deletions but were generally short, with a median of 1 bp for both the
209 Chr1 and Chr19 deletions (**Fig. S7A**). Thus, substantial microhomology is not required for joining.
210 However, the 24 recurring deletions on Chr1 had longer microhomologies with a median 6 bp (**Fig.
211 S7B**). Twelve of the recurring deletions arose within a 22/23-bp imperfect sequence repeat shared
212 between the two hotspots, and eight of these involved an 8-bp microhomology within the repeat (**Fig.
213 3C, S7B**). Thus, the availability and distribution of short sequence repeats likely influences deletion
214 outcomes.
215 The presence or absence of microhomologies within end-joining products may be indicative of
216 the end joining pathway used and/or processing at DNA ends. For example, SPO11-bound DSB ends
217 normally require endonucleolytic processing by MRE11 to release SPO11 oligos[4,41,42]. This may
218 disfavor canonical nonhomologous end-joining and promote alternative pathways that utilize
219 microhomology[43]. However, as some DSBs remain unresected in the absence of ATM/Tel1[30-34],
220 deletions may also arise from joining at or very close to SPO11 cleavage positions, which would
221 involve alternative SPO11 removal mechanisms, such as TDP2[30,44,45]. Our findings are thus consistent
222 with multiple end-joining mechanisms being employed to repair adjacent DSBs in the absence of
223 ATM.
224
225 **Insertion of hotspot-derived fragments**
226

227 Unexpectedly, we observed insertions in 11% of deletions from *Atm*$^{-/-}$ mice (27/243; two deletions
228 with two inserts, for 29 total inserts; **Table S1**). All but one of the inserted DNA fragments mapped to
229 chromosome positions showing SPO11 activity, either the assayed hotspot pairs themselves or other
230 hotspots. The insert that mapped to a sequence with no SPO11 oligos contained a CT-rich
231 microsatellite repeat and shared significant microhomology with both deletion breakpoints (12 and 9
232 bp) (**Table S3**), suggesting a possible DNA synthesis-based insertion mechanism.
233 ***Ectopic insertions from other hotspots***. Fifteen inserts of 15–349 bp mapped to other
234 chromosome positions at hotspots or SPO11-oligo clusters that were below the hotspot-calling
235 threshold (**Fig. 4A-C; S8, S9A; Table S3)**. Microhomologies at both sides of inserts were often short
236 (0 to 2 bp), similar to deletions without insertions (**Fig. 4D; Table S3**).
237 Most of these inserts could be uniquely mapped, however, three were derived from the non-
238 pseudoautosomal region (non-PAR) of the Y chromosome. The mouse non-PAR Y is highly
239 ampliconic[46], so these inserts cannot be assigned to a single location. Hotspots have been called at
240 some of these locations based on the assignment of unique SPO11 oligos, although most SPO11 oligos
241 map to multiple locations that are highly similar (**Fig. 4B,C; S9A; S10; Table S3**). Among all
242 chromosomes, the non-PAR Y experiences the largest increase in SPO11-oligo density in the absence
243 of ATM (~30 fold)[9].
244 Inserts mapped at or close to the hotspot/cluster centers, such that nearly half had an end within
245 50 bp (**Fig. 4B**). We envision that these inserts derive from DNA fragments released by SPO11 double
246 cutting. It seems remarkable that inserts can sometimes originate from SPO11-oligo clusters, i.e.,
247 genomic sites that are much less frequently targeted by SPO11 than called hotspots, as such weak sites
248 would be unlikely to experience two DSBs in the same cell if each DSB occurred independently at a
249 population-average frequency. However, these findings are readily explained by the recent observation
250 of concerted SPO11 cleavage within hotspots (especially in *Atm*$^{-/-}$)[47]. The ectopic insertion of SPO11-
251 generated fragments into other SPO11-generated DSB locations represents a novel pathway for
252 meiosis-specific, nonreciprocal genome modification by translocation of sequences.
253 ***Inverted insertions derived locally from the hotspot pair***. Twelve deletions had insertions of
254 16 to 709 bp that mapped to one of the hotspots but were reinserted in opposite orientation (inverted
255 insertions; **Fig. 4E; S9A,B**), including one with an inverted insertion from each hotspot in the pair.
256 Reconstructing the insertion breakpoints illuminated potential inversion mechanisms. Specifically, in
257 each case, one insertion breakpoint shared an inverted microhomology with one deletion breakpoint
258 (median 5 bp) (**Fig. 4F,G**). The other insertion breakpoint, which was at or near this deletion
259 breakpoint, had no or little microhomology with the other deletion breakpoint (median 0 bp). Inserts
260 from the left and right hotspots mirrored each other, i.e., those from the left hotspot had the longer
261 microhomology at the right breakpoint, whereas those from the right hotspot had the longer
262 microhomology at the left breakpoint (**Fig. 4E,G; S9B; Table S4**). Insert sequences clustered around
263 hotspot centers (**Fig. 4H**), indicating that they originated from DSB formation.
264 We propose two models to explain these events (**Fig. 4F**). In one, DSBs occur at or near the
265 two inverted microhomologies, creating a small double-cut fragment within one hotspot, and a third
266 DSB in the other hotspot generates a larger fragment destined for deletion. One end of the small
267 fragment remains unprocessed, preventing normal recombination at this hotspot, while both ends with
268 the inverted microhomology are at least partially resected, allowing strand annealing and fragment
269 inversion. The unprocessed end of the now inverted fragment joins to the third DSB at the other
270 hotspot. This is an attractive model because it incorporates defects seen in *Atm*$^{-/-}$ mice, i.e., impaired
271 DSB processing[30,31], as well as invoking closely spaced DSBs. In the second model, a DSB occurs next
272 to just one of the inverted microhomologies and resection exposes the second microhomology. A

foldback structure formed by annealing the inverted microhomologies is further processed by a structure-specific nuclease, generating a 5′ overhang that is filled in prior to joining the DSB end at the other hotspot. Foldback structures may be common in *Atm*$^{-/-}$, because the excess of DSBs may exhaust the pool of RPA[48], which normally prevents formation of secondary structures[49].

Interestingly, four inverted insertions from the right hotspot at the Chr1 hotspot pair involved the previously identified recurrent deletion site (**Fig. 3B; S9B**). In this case, 13 bp overlapping the recurrent deletion shares inverted microhomology with the most prominent DSB peak. Thus, this genomic location often engages in inappropriate repair (9% of all Chr1 deletions), demonstrating that DSB formation at or nearby such sequences may cause (mis)repair products to arise.

Microdeletions within a single hotspot

If more than one DSB can form inside the same hotspot, and not just at adjacent hotspots, we predicted that small deletions might also arise within single hotspots. The presumed origin of insertions from hotspot fragments implies that closely spaced DSBs can indeed occur within individual hotspots. We applied deep sequencing to test for such microdeletions. We selected a hotspot on Chr1 ranked among the five strongest in both *Atm*$^{-/-}$ and wild type. The SPO11-oligo profile for this hotspot displays a major central peak, a secondary peak, and several minor peaks, with SPO11 oligos spreading up to ~500 bp on both sides of the central peak, especially to the right (**Fig. 5A**). We designed four overlapping amplicons, ~580 bp each, to scan ~900 bp of the hotspot. This strategy would recover deletions around the major peak as well as those with one or both breakpoints away from the major peak, as often seen for inserts (**Fig. 4B**). Multiple, independent PCRs were carried out, each with input testis DNA equivalent to ~16,000 haploid genomes, for a total of ~10 million haploid genomes per amplicon. From pools of amplified DNA we sequenced ~3.5–5 million molecules per amplicon.

We identified reads containing microdeletions ranging from 11 to 229 bp (**Fig. 5A**). (Reads with ≤10-bp deletions were not considered; **Fig. S11A**). In *Atm*$^{-/-}$, 216 reads with microdeletions were detected from the four amplicons, for a total frequency of 1.58×10^{-5}, significantly greater than in *Spo11*$^{-/-}$ (0.19×10^{-5}), wild type (0.54×10^{-5}), and *Atm*$^{+/-}$ (0.23×10^{-5}) ($p<0.0001$, Chi square test) (**Table S4**). For some amplicons, reads from wild type and *Atm*$^{+/-}$ were also more frequent than in *Spo11*$^{-/-}$ (**Table S4**). If we disregard duplicate reads for a specific microdeletion from a given amplicon, we conservatively estimate that we obtained 149 independent microdeletions in total from *Atm*$^{-/-}$ (**Fig. 5A**). This is likely an underestimate since some microdeletions were found in multiple amplicons (**Fig. S11B**).

Microdeletion breakpoints frequently clustered at SPO11-oligo sites in *Atm*$^{-/-}$ (**Fig. 5A**). Prominent clusters were observed at the major SPO11-oligo peak (amplicons 1 to 3) and at the secondary SPO11-oligo peak (amplicons 1 to 4), indicating that microdeletions arose from SPO11-generated DSBs. This was even more evident when we pooled the 82 independent microdeletions from amplicons 1, 2, and 3 for which both breakpoints mapped within the 304-bp overlapping region (i.e., between the forward primer of amplicon 3 and the reverse primer of amplicon 1) (**Fig. 5B**). It was visually striking that many microdeletions had both breakpoints within these two SPO11-oligo peaks (17/82; 21%, 3 of which were recurring; **Fig. S11B**), implying that they originated from double cutting. In the smoothed breakpoint profiles, the most prominent left breakpoint peak matched the major SPO11-oligo peak, while the most prominent right breakpoint peak matched the secondary SPO11-oligo peak (**Fig. 5C**). These breakpoint peaks became even more prominent when all 116 reads in this overlap region were considered, something not seen with random sampling of reads (**Fig. S11C**). Thus, at least some of the duplicated reads likely represent independent microdeletions.

319 Microdeletions in the overlap region displayed a distinct length distribution (**Fig. 5D**), with two
320 prominent microdeletion classes of ~30 bp and ~60 bp. The ~60-bp microdeletions predominantly
321 mapped between the major SPO11-oligo peak and the secondary SPO11-oligo peak (71%, 17/24 from
322 49–70 bp; **Fig. 5E**), which are separated by 55 bp (**Fig. 5C**); reads within this class were often
323 duplicated (**Fig. S12A**). A subset of the ~30-bp microdeletions (22%, 4/18 from 27–42 bp; **Fig. 5E**)
324 mapped between a minor SPO11-oligo peak and the secondary SPO11-oligo peak 34 bp away (**Fig.**
325 **5C**). These results imply that hotspot substructure predicts double cutting and, hence, microdeletion
326 locations. Conversely, double cutting will affect SPO11-oligo distribution within a hotspot when
327 SPO11 oligos predominantly arise from double cutting.
328 In addition to microdeletions between two SPO11-oligo peaks, ~30-bp (56%, 10/18) and ~60-
329 bp (21%, 5/24) microdeletions often had only one breakpoint at a SPO11-oligo peak (**Fig. 5E**).
330 Assuming they also arose from two SPO11 breaks, the distinct size classes may reflect a more general
331 underlying mechanism for double cutting, such that the length of double-cut fragments may be
332 constrained. In that case, it remains possible that some of the ~60-bp microdeletions may have arisen
333 from two double cuts (triple cutting), releasing two ~30-bp fragments, rather than a single double cut,
334 although this may be less likely given that very few of the ~30-bp microdeletions have left breakpoints
335 within the major SPO11-oligo peak like the ~60-bp microdeletions.
336 Microdeletions, especially the ~60-bp class, frequently removed the PRDM9 binding site,
337 which is located between the major and secondary SPO11-oligo peaks (**Fig. 5E**). PRDM9 binding
338 could potentially affect the spacing of double cuts. However, as similar microdeletion lengths are
339 observed outside the PRDM9 motif, another or additional factors must exist that lead to this size class.
340 Interestingly, the major SPO11-oligo peak and the adjacent minor peak are separated by 21 bp
341 (**Fig. 5C**), but the few small microdeletions (11–24 bp) did not map between these peaks (**Fig. 5D, E**),
342 implying that two SPO11-induced DSBs may be constrained to longer distances. Thus, it is possible
343 that they originated from single DSBs or even from double cuts with partial gap filling.
344 A less prominent microdeletion class of ~140 bp was also observed (129–153 bp, **Fig. 5D**). In
345 several of these longer microdeletions, the left breakpoint clustered at the major SPO11-oligo peak,
346 whereas the right breakpoint was located at sites in which fewer SPO11 oligos mapped (46%, 6/13;
347 **Fig. 5E**). These longer microdeletions may also arise from double cutting. Long SPO11 oligos are
348 observed in *Atm*$^{-/-}$ testes[4], but are underrepresented in SPO11-oligo maps, given the size selection
349 during library preparation[9,50]. Even longer microdeletions were also observed that peaked at ~180 bp
350 and ~230 bp (**Fig. 5D**), especially when considering all amplicons where microdeletions were less
351 sized constrained (**Fig. S12B,C**). Some of these long microdeletions may have arisen from multiple
352 double-cut fragments that generated long gaps. However, it is notable that the median insert size from
353 other hotspots in the paired hotspot deletions was quite long (~100 bp), with one insert extending 349
354 bp, suggesting that long double-cut fragments can be generated.
355 In *Atm*$^{+/+}$ and *Atm*$^{+/-}$, microdeletions did not display obvious spatial patterns (**Fig. 5A,E**).
356 Because the frequency of microdeletions in the presence of ATM is only slightly higher in some
357 amplicons than in *Spo11*$^{-/-}$, we consider that a portion of these events arose from PCR errors or other
358 genomic damage, as in *Spo11*$^{-/-}$. Strikingly, however, a ~30-bp (25–43-bp) microdeletion class was
359 also apparent, but not in the *Spo11*$^{-/-}$ control, although the prominent ~60-bp microdeletion class found
360 in *Atm*$^{-/-}$ was not observed (**Fig. 5D, S12B**). Microdeletions from the ~30-bp class did not map within
361 SPO11-oligo peaks, although some breakpoints clustered (**Fig. 5E**). Possibly, in the presence of ATM,
362 microdeletions are more likely to occur at DSBs formed outside of SPO11-oligo peaks. In both the
363 presence and absence of ATM, microhomology at breakpoints was generally short (median 1 bp) (**Fig.**
364 **S12D**), similar to deletions between hotspot pairs.

Our assumption that SPO11 double cutting occurs within individual hotspots, preceding microdeletion formation, is consistent with recent findings from *S. cerevisiae* in which double-cut fragments were observed[47,51]. Their minimum size was determined to be ~30 bp but longer fragments in increments of ~10 bp were abundant as well. The authors suggest models in which Spo11 is constrained to make the simultaneous cleavages. The recent finding of condensates of the yeast DSB repair machinery suggests a mechanism whereby centers of DSB activity form which could provide such a platform[52]. Our single hotspot data fit well with both of these concepts. Further, Johnson et al. computationally identified potential SPO11 double-cut fragments within mouse hotspots in SPO11-oligo libraries[9]. Assuming a similar lower size limit in mouse as in yeast, double-cut fragments are predicted to peak at ~32 bp and extend to ≤60 bp in *Atm*$^{-/-}$, near the size limit of the SPO11-oligo library preparation[9]. Our analysis of microdeletions is in line with this finding, given a prominent microdeletion class of ~30 bp, but also suggests that SPO11-oligo double-cut fragments extend much longer, i.e., from ≥60 bp to at least ~230 bp, congruent with the observation of long SPO11 oligos in *Atm*$^{-/-}$[4].

Conclusions

Our study uncovers *de novo* deletions in the mouse germline arising at DNA gaps generated by SPO11 double cutting and repaired by nonhomologous end-joining Although pronounced in the absence of ATM, deletions and microdeletions also occur at low frequency in the presence of ATM. Deletions in both our hotspot pairs remove exons, demonstrating that SPO11-mediated deletions can disrupt gene function and/or produce new alleles. Importantly, short direct and inverted repeats at DSB hotspots help drive these events. The occurrence of deletions involving two chromosomes also predicts gross rearrangements. Thus, these deletions reveal a previously hidden potential in meiosis for mutagenesis and the disruption of genome integrity. Furthermore, double-cut fragments appear to be released from hotspots and inserted at other genomic sites undergoing DSBs, also with mutagenic consequences. Because DNA gaps are thought to initiate a subset of meiotic recombination events as part of the normal meiotic program[47], this raises the question as to how re-insertion of released double-cut fragments is usually suppressed.

Microdeletions resulted in PRDM9 motif deletion in 38% of events in the absence of ATM and 11% in the presence of ATM. By eliminating PRDM9 motifs, such deletions shape the recombination landscape, thus influencing genome evolution[53,54] and potentially contributing to speciation[55,56]. Because PRDM9 drives recombination away from promoters[57], deletions may be better tolerated in PRDM9-dependent meiotic recombination, including in humans, and in turn have a greater potential impact on human genome evolution.

Acknowledgments

We thank Matthew Neale and Franz Klein for sharing unpublished results; members of the Jasin and Keeney labs for assistance and discussions, in particular Shintaro Yamada; and MSK core facilities, in particular the Integrated Genomics Operation (Cassidy Cobbs, Neeman Mohibullah, Agnès Viale) and the Bioinformatics Core (Nicholas Socci), which are supported by NIH grant P30 CA008748. This work was supported by March of Dimes grant 1-FY17-799 (A.L.), American Cancer Society fellowship PF-12-157-01-DMC (J.L.), NIH grant R35 GM118092 (S.K.), and NIH grant R35 GM118175 (M.J.).

Author contributions

A.L., S.K., and M.J. conceived the research and designed the experiments with contributions from J.L. A.L. performed all of the experiments. A.L. and M.J. wrote the manuscript with input from S.K. and J.L.

Ethics declarations

Competing interests

The authors declare no competing interests.

References

1 de Massy, B. Initiation of meiotic recombination: how and where? Conservation and specificities among eukaryotes. *Annu Rev Genet* **47**, 563-599, doi:10.1146/annurev-genet-110711-155423 (2013).

2 Hunter, N. Meiotic Recombination: The Essence of Heredity. *Cold Spring Harb Perspect Biol* **7**, doi:10.1101/cshperspect.a016618 (2015).

3 Keeney, S., Lange, J. & Mohibullah, N. Self-organization of meiotic recombination initiation: general principles and molecular pathways. *Annu Rev Genet* **48**, 187-214, doi:10.1146/annurev-genet-120213-092304 (2014).

4 Lange, J. *et al.* ATM controls meiotic double-strand-break formation. *Nature* **479**, 237-240, doi:10.1038/nature10508 (2011).

5 Lukaszewicz, A., Lange, J., Keeney, S. & Jasin, M. Control of meiotic double-strand-break formation by ATM: local and global views. *Cell Cycle* **17**, 1155-1172, doi:10.1080/15384101.2018.1464847 (2018).

6 Keeney, S. Mechanism and control of meiotic recombination initiation. *Curr Top Dev Biol* **52**, 1-53 (2001).

7 Petes, T. D. Meiotic recombination hot spots and cold spots. *Nat Rev Genet* **2**, 360-369, doi:10.1038/35072078 (2001).

8 Baudat, F., Imai, Y. & de Massy, B. Meiotic recombination in mammals: localization and regulation. *Nat Rev Genet* **14**, 794-806, doi:10.1038/nrg3573 (2013).

9 Lange, J. *et al.* The Landscape of Mouse Meiotic Double-Strand Break Formation, Processing, and Repair. *Cell* **167**, 695-708 e616, doi:10.1016/j.cell.2016.09.035 (2016).

10 Cole, F. *et al.* Homeostatic control of recombination is implemented progressively in mouse meiosis. *Nat Cell Biol* **14**, 424-430, doi:10.1038/ncb2451 (2012).

11 Tock, A. J. & Henderson, I. R. Hotspots for Initiation of Meiotic Recombination. *Front Genet* **9**, 521, doi:10.3389/fgene.2018.00521 (2018).

12 Pan, J. *et al.* A hierarchical combination of factors shapes the genome-wide topography of yeast meiotic recombination initiation. *Cell* **144**, 719-731, doi:10.1016/j.cell.2011.02.009 (2011).

456 13 Yamada, S. *et al.* Genomic and chromatin features shaping meiotic double-strand break
457 formation and repair in mice. *Cell Cycle* **16**, 1870-1884, doi:10.1080/15384101.2017.1361065
458 (2017).
459 14 Cooper, T. J., Garcia, V. & Neale, M. J. Meiotic DSB patterning: A multifaceted process. *Cell*
460 *Cycle* **15**, 13-21, doi:10.1080/15384101.2015.1093709 (2016).
461 15 Shiloh, Y. The ATM-mediated DNA-damage response: taking shape. *Trends Biochem Sci* **31**,
462 402-410, doi:10.1016/j.tibs.2006.05.004 (2006).
463 16 Tian, M. & Loidl, J. A chromatin-associated protein required for inducing and limiting meiotic
464 DNA double-strand break formation. *Nucleic Acids Res* **46**, 11822-11834,
465 doi:10.1093/nar/gky968 (2018).
466 17 Checchi, P. M., Lawrence, K. S., Van, M. V., Larson, B. J. & Engebrecht, J. Pseudosynapsis
467 and decreased stringency of meiotic repair pathway choice on the hemizygous sex chromosome
468 of Caenorhabditis elegans males. *Genetics* **197**, 543-560, doi:10.1534/genetics.114.164152
469 (2014).
470 18 Mohibullah, N. & Keeney, S. Numerical and spatial patterning of yeast meiotic DNA breaks by
471 Tel1. *Genome Res* **27**, 278-288, doi:10.1101/gr.213587.116 (2017).
472 19 Garcia, V., Gray, S., Allison, R. M., Cooper, T. J. & Neale, M. J. Tel1(ATM)-mediated
473 interference suppresses clustered meiotic double-strand-break formation. *Nature* **520**, 114-118,
474 doi:10.1038/nature13993 (2015).
475 20 Chang, H. H. Y., Pannunzio, N. R., Adachi, N. & Lieber, M. R. Non-homologous DNA end
476 joining and alternative pathways to double-strand break repair. *Nat Rev Mol Cell Biol* **18**, 495-
477 506, doi:10.1038/nrm.2017.48 (2017).
478 21 Kim, S., Peterson, S. E., Jasin, M. & Keeney, S. Mechanisms of germ line genome instability.
479 *Semin Cell Dev Biol* **54**, 177-187, doi:10.1016/j.semcdb.2016.02.019 (2016).
480 22 Ahmed, E. A., Philippens, M. E., Kal, H. B., de Rooij, D. G. & de Boer, P. Genetic probing of
481 homologous recombination and non-homologous end joining during meiotic prophase in
482 irradiated mouse spermatocytes. *Mutat Res* **688**, 12-18, doi:10.1016/j.mrfmmm.2010.02.004
483 (2010).
484 23 Ahmed, E. A., Rosemann, M. & Scherthan, H. NHEJ Contributes to the Fast Repair of
485 Radiation-induced DNA Double-strand Breaks at Late Prophase I Telomeres. *Health Phys* **115**,
486 102-107, doi:10.1097/HP.0000000000000852 (2018).
487 24 Enguita-Marruedo, A. *et al.* Transition from a meiotic to a somatic-like DNA damage response
488 during the pachytene stage in mouse meiosis. *PLoS Genet* **15**, e1007439,
489 doi:10.1371/journal.pgen.1007439 (2019).
490 25 Girard, C., Roelens, B., Zawadzki, K. A. & Villeneuve, A. M. Interdependent and separable
491 functions of Caenorhabditis elegans MRN-C complex members couple formation and repair of
492 meiotic DSBs. *Proc Natl Acad Sci U S A* **115**, E4443-E4452, doi:10.1073/pnas.1719029115
493 (2018).
494 26 Lemmens, B. B., Johnson, N. M. & Tijsterman, M. COM-1 promotes homologous
495 recombination during Caenorhabditis elegans meiosis by antagonizing Ku-mediated non-
496 homologous end joining. *PLoS Genet* **9**, e1003276, doi:10.1371/journal.pgen.1003276 (2013).
497 27 Yin, Y. & Smolikove, S. Impaired resection of meiotic double-strand breaks channels repair to
498 nonhomologous end joining in Caenorhabditis elegans. *Mol Cell Biol* **33**, 2732-2747,
499 doi:10.1128/MCB.00055-13 (2013).
500 28 Macaisne, N., Kessler, Z. & Yanowitz, J. L. Meiotic Double-Strand Break Proteins Influence
501 Repair Pathway Utilization. *Genetics* **210**, 843-856, doi:10.1534/genetics.118.301402 (2018).

29 Martin, J. S., Winkelmann, N., Petalcorin, M. I., McIlwraith, M. J. & Boulton, S. J. RAD-51-dependent and -independent roles of a Caenorhabditis elegans BRCA2-related protein during DNA double-strand break repair. *Mol Cell Biol* **25**, 3127-3139, doi:10.1128/MCB.25.8.3127-3139.2005 (2005).
30 Paiano, J. *et al.* ATM and PRDM9 regulate SPO11-bound recombination intermediates during meiosis. *Nat Commun* **11**, 857, doi:10.1038/s41467-020-14654-w (2020).
31 Yamada, S. *et al.* Molecular structures and mechanisms of DNA break processing in mouse meiosis. *Genes Dev*, doi:10.1101/gad.336032.119 (2020).
32 Mimitou, E. P., Yamada, S. & Keeney, S. A global view of meiotic double-strand break end resection. *Science* **355**, 40-45, doi:10.1126/science.aak9704 (2017).
33 Cannavo, E. *et al.* Regulatory control of DNA end resection by Sae2 phosphorylation. *Nat Commun* **9**, 4016, doi:10.1038/s41467-018-06417-5 (2018).
34 Joshi, N., Brown, M. S., Bishop, D. K. & Borner, G. V. Gradual implementation of the meiotic recombination program via checkpoint pathways controlled by global DSB levels. *Mol Cell* **57**, 797-811, doi:10.1016/j.molcel.2014.12.027 (2015).
35 Barlow, C. *et al.* Atm deficiency results in severe meiotic disruption as early as leptonema of prophase I. *Development* **125**, 4007-4017 (1998).
36 Xu, Y. *et al.* Targeted disruption of ATM leads to growth retardation, chromosomal fragmentation during meiosis, immune defects, and thymic lymphoma. *Genes Dev* **10**, 2411-2422, doi:10.1101/gad.10.19.2411 (1996).
37 Cole, F., Keeney, S. & Jasin, M. Comprehensive, fine-scale dissection of homologous recombination outcomes at a hot spot in mouse meiosis. *Mol Cell* **39**, 700-710, doi:10.1016/j.molcel.2010.08.017 (2010).
38 Marsolier-Kergoat, M. C., Khan, M. M., Schott, J., Zhu, X. & Llorente, B. Mechanistic View and Genetic Control of DNA Recombination during Meiosis. *Mol Cell* **70**, 9-20 e26, doi:10.1016/j.molcel.2018.02.032 (2018).
39 Anderson, C. M., Oke, A., Yam, P., Zhuge, T. & Fung, J. C. Reduced Crossover Interference and Increased ZMM-Independent Recombination in the Absence of Tel1/ATM. *PLoS Genet* **11**, e1005478, doi:10.1371/journal.pgen.1005478 (2015).
40 Zhang, L., Kim, K. P., Kleckner, N. E. & Storlazzi, A. Meiotic double-strand breaks occur once per pair of (sister) chromatids and, via Mec1/ATR and Tel1/ATM, once per quartet of chromatids. *Proc Natl Acad Sci U S A* **108**, 20036-20041, doi:10.1073/pnas.1117937108 (2011).
41 Keeney, S., Giroux, C. N. & Kleckner, N. Meiosis-specific DNA double-strand breaks are catalyzed by Spo11, a member of a widely conserved protein family. *Cell* **88**, 375-384, doi:10.1016/s0092-8674(00)81876-0 (1997).
42 Neale, M. J., Pan, J. & Keeney, S. Endonucleolytic processing of covalent protein-linked DNA double-strand breaks. *Nature* **436**, 1053-1057, doi:10.1038/nature03872 (2005).
43 Sfeir, A. & Symington, L. S. Microhomology-Mediated End Joining: A Back-up Survival Mechanism or Dedicated Pathway? *Trends in biochemical sciences* **40**, 701-714, doi:10.1016/j.tibs.2015.08.006 (2015).
44 Alvarez-Quilon, A. *et al.* ATM specifically mediates repair of double-strand breaks with blocked DNA ends. *Nat Commun* **5**, 3347, doi:10.1038/ncomms4347 (2014).
45 Johnson, D., Allison, R. M., Cannavo, E., Cejka, P. & Neale, M. J. Removal of Spo11 from meiotic DNA breaks in vitro but not in vivo by Tyrosyl DNA Phosphodiesterase 2. *bioRxiv*, doi:0.1101/527333 (2019).

46 Soh, Y. Q. *et al.* Sequencing the mouse Y chromosome reveals convergent gene acquisition and amplification on both sex chromosomes. *Cell* **159**, 800-813, doi:10.1016/j.cell.2014.09.052 (2014).
47 Johnson, D. *et al.* Concerted cutting by Spo11 illuminates DNA break mechanisms and initiates gap repair during meiosis. *bioRxiv*, doi:10.1101/2019.12.18.881268 (2019).
48 Toledo, L. I. *et al.* ATR prohibits replication catastrophe by preventing global exhaustion of RPA. *Cell* **155**, 1088-1103, doi:10.1016/j.cell.2013.10.043 (2013).
49 Deng, S. K., Chen, H. & Symington, L. S. Replication protein A prevents promiscuous annealing between short sequence homologies: Implications for genome integrity. *Bioessays* **37**, 305-313, doi:10.1002/bies.201400161 (2015).
50 Thacker, D., Mohibullah, N., Zhu, X. & Keeney, S. Homologue engagement controls meiotic DNA break number and distribution. *Nature* **510**, 241-246, doi:10.1038/nature13120 (2014).
51 Prieler, S. *et al.* Spo11 generates chromosomal gaps through concerted cuts and targets sites of topological stress. (Submitted).
52 Claeys Bouuaert, C., Pu, S., Wang, J., Patel, D. J. & Keeney, S. DNA-dependent macromolecular condensation drives self-assembly of the meiotic DNA break machinery. *bioRxiv*, doi:10.1101/2020.02.21.960245 (2020).
53 Cole, F. *et al.* Mouse tetrad analysis provides insights into recombination mechanisms and hotspot evolutionary dynamics. *Nat Genet* **46**, 1072-1080, doi:10.1038/ng.3068 (2014).
54 Baker, C. L. *et al.* PRDM9 drives evolutionary erosion of hotspots in Mus musculus through haplotype-specific initiation of meiotic recombination. *PLoS Genet* **11**, e1004916, doi:10.1371/journal.pgen.1004916 (2015).
55 Davies, B. *et al.* Re-engineering the zinc fingers of PRDM9 reverses hybrid sterility in mice. *Nature* **530**, 171-176, doi:10.1038/nature16931 (2016).
56 Smagulova, F., Brick, K., Pu, Y., Camerini-Otero, R. D. & Petukhova, G. V. The evolutionary turnover of recombination hot spots contributes to speciation in mice. *Genes Dev* **30**, 266-280, doi:10.1101/gad.270009.115 (2016).
57 Brick, K., Smagulova, F., Khil, P., Camerini-Otero, R. D. & Petukhova, G. V. Genetic recombination is directed away from functional genomic elements in mice. *Nature* **485**, 642-645, doi:10.1038/nature11089 (2012).

Methods

Mouse husbandry

All experiments were conducted according to US Office of Laboratory Animal Welfare regulatory standards and were approved by the Memorial Sloan Kettering Cancer Center Institutional Animal Care and Use Committee. Mice were purchased from The Jackson Laboratory where indicated. *Atm*$^{+/-}$ males on the C57BL/6J (B6) background (B6.129S6-*Atm*^{tm1Awb}/J; stock #008536) were crossed with B6 females (stock #000664) to establish a breeding colony and to obtain experimental animals. The *Atm* mutation was previously described[58]. *Atm*$^{+/-}$ B6 mice were crossed with *Atm*$^{+/-}$ DBA/2J (DBA) mice to get F1 hybrid males. *Atm*$^{+/-}$ mice on the DBA background were obtained by six backcrosses of *Atm*$^{+/-}$ mice that were partially on an A/J background with DBA inbred mice (stock #000671). Animals were fed regular rodent chow with continuous access to food and water.

594
595 **Isolation of testis genomic DNA**
596
597 DNA was isolated from testicular single-cell suspensions to enrich for germ cells. Testis dissociation
598 was based on protocols previously described[53,59] with some modifications. Testes from juvenile 15-
599 day-old and adult 2- to 5-month-old mice were decapsulated and seminiferous tubules incubated at 33
600 °C in 10 ml Gey's Balanced Salt Solution (GBSS) (Sigma) with 0.5 mg/ml collagenase (Sigma) and 2
601 μg/ml DNase I (Roche) for 15–20 min, shaking at 500 rpm. After 10 min and at the end of the
602 incubation the tubules were gently pipetted up and down using a transfer pipette. The tubules were
603 washed twice with 10 ml GBSS and digested with 0.5 mg/ml trypsin (Sigma) in 10 ml GBSS,
604 supplemented with 2 μg/ml DNase I, for 25–40 min at 33 °C, shaking at 500 rpm. Pipetting up and
605 down was performed at the start, midpoint and end of the incubation. Trypsin was inhibited by adding
606 10% fetal calf serum. Cell suspension was obtained by repeated pipetting for 2 min and filtration
607 through a 70-μm cell strainer (ThermoFisher). All of the mutant cell suspension and one-third to one-
608 half of the wild-type cell suspension was transferred to a 15 ml tube and centrifuged for 3 min at 1550
609 × g. The cell pellet was resuspended by tapping the tube, followed by the addition of 600 μl lysis
610 buffer (200 mM NaCl, 100 mM Tris-Cl pH 7.5, 5 mM EDTA, 0.5% SDS, 0.5 mg/ml Proteinase K).
611 The lysate was transferred to a 1.5 ml Eppendorf tube and incubated overnight at 55 °C. Genomic
612 DNA was isolated using phenol-chloroform extraction and alcohol precipitation, with the extraction
613 step repeated twice. DNA was dissolved in 200–400 μl H_2O, incubated for 1 h at 55 °C and overnight
614 at 4 °C. DNA concentration was quantified by NanoDrop (ThermoFisher). DNA was diluted to ~200
615 ng/μl and incubated for another 2–3 h at 37 °C to reduce the viscosity of the DNA solution. DNA
616 concentration was measured again three times before freezing. DNA samples were stored at -20 °C.
617
618 **Detection of deletions at hotspot pairs by nested PCR**
619
620 Deletions were detected by nested PCR using primers flanking the two hotspots of a pair (**Fig. 1B;**
621 **S2A**). Prior to PCR, genomic DNA was digested with restriction enzymes where indicated to suppress
622 parental DNA amplification (**Fig. S4**). Restriction digestions were performed in a 60 μl volume with
623 1200 ng of DNA and 4–4.5 μl restriction enzyme(s) (Chr1 hotspot pair: NsiI, NcoI, and BglII or NcoI
624 alone; Chr19 hotspot pair: BamHI or KpnI). Reactions were incubated overnight at 37 °C followed by
625 an additional 3 h of incubation with a 1.5–2 μl of fresh restriction enzyme(s), then placed on ice before
626 PCR. In the majority of PCRs, 2.5 μl of the digestion reaction was used per PCR, equivalent to 50 ng
627 of genomic DNA, with this DNA concentration being optimal for the estimation of deletion
628 frequencies; 1.25 μl and 5 μl, equivalent to 25 ng and 100 ng, respectively, were also tested. In the
629 experiments with no digestion, 50 ng of DNA template was used per PCR in most cases.
630 Nested PCR was based on the previously described protocol[60] with some adjustments. A first
631 round of PCR was performed using the following primers: Chr1_DH_FW1: 5′-
632 GGTCAGGAGGATGGGGAG-3′ and Chr1_DH_RV1: 5′-CCAAGAAGGTGCTTATCGTCC-3′ for
633 the Chr1 hotspot pair, Chr19_DH_FW2: 5′-TGGAATGTAGCCTCTGGCAG-3′ and Chr19_DH_RV2:
634 5′-GTGCTGTCAGAAGCCGTGG-3′ for the Chr19 hotspot pair, Chr1_DH_DB_FW1: 5′-
635 CCTGGAGACCAAAGCCAC-3′ and Chr1_DH_RV1: 5′-CCAAGAAGGTGCTTATCGTCC-3′ for
636 the Chr1 hotspot pair in B6/DBA F1 hybrids. A second round of PCR was performed using the
637 following primers: Chr1_DH_FW2: 5′-GCCTTGGCTCAAAGTGTCTG-3′ and Chr1_DH_RV2: 5′-
638 TCCCTTCTGCCATCCTTCTG-3′ for the Chr1 hotspot pair, newChr19_DH_FW2: 5′-

639 CCCAAAGTTGTCCTTGCTTCC-3′ and newChr19_DH_RV2: 5′-TGGTTTCCAGAGGAGAGGAC-
640 3′ for the Chr19 hotspot pair, Chr1_DH_DB_FW2: 5′-GGCATTGCTTCATTCATGGTCTG-3′ and
641 Chr1_DH_RV2-3: 5′-CATTGTCATCTTGAGCACTCCTC-3′ for the Chr1 hotspot pair in B6/DBA
642 F1 hybrids. The annealing temperature was optimized for each primer pair by gradient PCR with testis
643 genomic DNA of known high quality. DNA samples from different testes were also tested for the
644 appearance of a strong parental PCR band using the primary PCR primers.
645 For nested PCR, each primary PCR was performed in a 50 μl volume containing: 1x Jeffreys
646 buffer (10x: 450 mM Tris-Cl pH 8.8, 110 mM $(NH_4)_2SO_4$, 45 mM $MgCl_2$, 67 mM 2-mercaptoethanol,
647 44 μM EDTA, 10 mM each dNTP (Roche), 1.13 mg/ml ultra-pure (non-acetylated) BSA (Ambion),
648 12.5 mM Tris base), 0.2 μM primers, 0.03 U/μl Taq DNA polymerase (ThermoFisher) and 0.006 U/μl
649 Pfu Turbo DNA polymerase (Agilent). The primary PCR product (0.6 μl) was treated with S1 nuclease
650 (ThermoFisher) at room temperature for 30 min, in a 5 μl volume containing: 0.5x S1 buffer, 0.2 U/μl
651 S1 nuclease and 5 ng/μl sonicated salmon sperm DNA. The reaction was diluted with 45 μl of dilution
652 buffer (10 mM Tris-Cl pH 7.5 and 5 ng/μl sonicated salmon sperm DNA). 4 μl of the diluted S1
653 reaction was seeded into the secondary PCR, which was performed in a 20 μl volume containing the
654 same components as the primary PCR. Deletion products were identified by electrophoresis on a 1%
655 agarose gel (**Fig. 1C, Fig. S2B**). PCR products smaller than the parental size were excised, purified,
656 and Sanger sequenced using primers from the second round of PCR and in some cases additional
657 primers. Diluted S1 reactions were stored at -20 °C, and used again for secondary PCRs if more PCR
658 product was needed for sequencing.
659 PCR conditions were tested for each hotspot pair. The best result, that is, the appearance of
660 more intense, smaller PCR products, was obtained when the extension time was shortened (<60 s/kb)
661 in the primary PCR to inhibit amplification of the longer parental PCR product. The extension time in
662 the secondary PCR was slightly shorter.
663 Primary PCR conditions were denaturation at 96 °C for 2 min, followed by 37 cycles of
664 amplification as follows: denaturation at 96 °C for 20 s, annealing at 59 °C for 30 s, extension at 65 °C
665 for 2 min for the Chr1 and Chr19 hotspot pairs (3.6 kb parental products), and 2 min 30 s for the Chr1
666 hotspot pair in B6/DBA hybrids (4 kb parental product). Secondary PCR conditions where the same,
667 but with different extension times: 3 min for the Chr1 and Chr19 hotspot pairs (3.4-kb parental
668 products) and 3 min 30 s for the Chr1 hotspot pair in B6/DBA hybrids (3.9-kb parental products).
669 Sequenced PCR products were analyzed using ApE software
670 (https://jorgensen.biology.utah.edu/wayned/ape/) to identify deletions, microhomologies, and
671 polymorphisms in DNA sequences. Deletion breakpoint profiling was performed using R versions
672 3.4.4 to 3.6.3 (http://www.r-project.org). Graphing was performed in R and GraphPad Prism version 8.
673
674 **Detection of microdeletions at a single hotspot by amplicon deep sequencing**
675
676 Four ~580-bp overlapping amplicons of the hotspot (**Fig. 5A**) were amplified using the following
677 primer pairs: amplicon 1, Chr1_MiSeq_FW1: 5′-TCATGTCCGGTTTGGATGCC-3′ and
678 Chr1_MiSeq_RV1: 5′-CGAATCAAAGACTCCAGAAGAGG-3′; amplicon 2, Chr1_MiSeq_FW2: 5′-
679 AGTAGCAAGAAGGGCTGGAG-3′ and Chr1_MiSeq_RV2: 5′-
680 AGAGACAGATGTGGAGGCTAAC-3′; amplicon 3, Chr1_MiSeq_FW4: 5′-
681 CTGAATCTCTCCTGGTGTGTC-3′ and Chr1_MiSeq_RV4: 5′-
682 AGGACATTGAATGTTTTTATGGTTC-3′; amplicon 4, Chr1_MiSeq_FW5: 5′-
683 AAACAGAAGAAGCAGTAATGCC-3′ and Chr1_MiSeq_RV5: 5′-

684 GTGTGCAACTGGGTATATTTCAG-3′. For each primer pair the annealing temperature was tested
685 by gradient PCR with testis genomic DNA of known high quality. To minimize PCR bias and jackpot
686 amplification of single deletion events, the number of amplification cycles was determined by when a
687 faint PCR product was first visible, which was 22 cycles for all samples. For each amplicon, PCR
688 conditions were the same: 96 °C for 2 min followed by 22 cycles at 96 °C for 20 s, 59 °C for 30 s and
689 65 °C for 35 s. PCR was performed in a 50 μl total containing 1.5 U Taq DNA polymerase
690 (ThermoFisher) and 0.3 U Pfu Turbo DNA polymerase (Agilent) in the Jeffreys buffer described above
691 for nested PCR with 50 ng of testis genomic DNA. Testis DNA was derived from 3-5 different mice
692 for each genotype and amplified independently.
693 PCRs were carried out in 96-well plates to generate a large number of independently-derived
694 PCR products for sequencing. For each amplicon, 576 PCRs were performed with a total of 28.8 μg
695 genomic DNA, equivalent to 9.6 million haploid genomes. PCRs were pooled, and a 1200-μl aliquot
696 was purified and concentrated on spin columns (Invitrogen PureLink™ PCR Purification Kit) as
697 follows: For each 100 μl PCR aliquot, 400 μl binding buffer from the kit was added, and then the
698 sample was applied to the column and centrifuged. This step was repeated 6 times in each of two
699 columns before washing and elution with 37 μl elution buffer. Eluted DNA was combined from the
700 two columns and a 15-μl aliquot was run on a 2% agarose gel to estimate DNA concentration, which
701 was ~2 ng/μl. The remaining ~60 μl was submitted to the Integrated Genomics Operation at MSK for
702 library preparation and deep sequencing. The library was prepared by ligation of indexed adapter
703 sequences using the KAPA HyperPrep Kit (Roche). Sequencing was performed using Illumina MiSeq
704 (2 x 300-bp paired-end reads). In a single run, libraries from amplicons 1–4 were mixed with 5% PhiX
705 DNA control library (Illumina) and sequenced. Because MiSeq can deliver 15–20 million reads per
706 lane, in our experiment, 3.6–4.8 million reads per amplicon were estimated, which was about 2 times
707 lower than the 9.6 million input DNA templates. With that calculation, not all deletion events were
708 recovered, but most recovered deletions should have yielded only a single read.
709 We performed 4 MiSeq runs with amplicons from different genotypes (**Fig. S11A**). FASTQ
710 sequencing files were analyzed using CRISPResso2[61,62] by the Bioinformatics Core Facility at MSK.
711 Reads were aligned to the reference amplicon sequence and 2.9–5.3 million paired-end reads were
712 mapped per amplicon. Alignments matching the target sequence for the first 20 and last 20 bases and
713 with one deletion event were filtered. Reads with >1 bp deletion and with no mutations in the sequence
714 were analyzed in R and ApE. Breakpoint distribution analyses and random sampling (**Fig. 11C**) were
715 performed in R. Graphs were plotted using R and GraphPad Prism, and the Chi-square test was
716 performed in GraphPad Prism.
717
718 **SPO11-oligo maps**
719
720 SPO11-oligo maps were generated previously (GEO accession number GSE84689)[9]. Mice for the *Atm*$^{-}$
721 $^{/-}$ data set "*Atm* null 1", which was used in all the analyses, were on a mixed B6 and 129/Sv strain
722 background. Two *Atm*$^{+/+}$ data sets are available, "B6", from mice on a pure B6 background, and "*Atm*
723 wt", from the same colony as *Atm*$^{-/-}$ mice. Hotspots selected in this study were called in the "B6" data
724 set (**Fig. 1B, S1D, S2A**), while analysis of hotspot distributions was done with the "*Atm* wt" data set
725 (**Fig. 1A, S1A–C**). The "B6" data set was also used to check if SPO11 oligos map to the genomic
726 locations from which inserts derived (**Fig. S8, S10**).
727
728 58 Barlow, C. *et al.* Atm-deficient mice: a paradigm of ataxia telangiectasia. *Cell* **86**, 159-171,
729 doi:10.1016/s0092-8674(00)80086-0 (1996).

730 59 Gaysinskaya, V., Soh, I. Y., van der Heijden, G. W. & Bortvin, A. Optimized flow cytometry
731 isolation of murine spermatocytes. *Cytometry A* **85**, 556-565, doi:10.1002/cyto.a.22463 (2014).
732 60 Cole, F. & Jasin, M. Isolation of meiotic recombinants from mouse sperm. *Methods Mol Biol*
733 **745**, 251-282, doi:10.1007/978-1-61779-129-1_15 (2011).
734 61 Clement, K. *et al.* CRISPResso2 provides accurate and rapid genome editing sequence analysis.
735 *Nat Biotechnol* **37**, 224-226, doi:10.1038/s41587-019-0032-3 (2019).
736 62 Pinello, L. *et al.* Analyzing CRISPR genome-editing experiments with CRISPResso. *Nat*
737 *Biotechnol* **34**, 695-697, doi:10.1038/nbt.3583 (2016).
738 63 Schirmer, M. *et al.* Insight into biases and sequencing errors for amplicon sequencing with the
739 Illumina MiSeq platform. *Nucleic Acids Res* **43**, e37, doi:10.1093/nar/gku1341 (2015).

Figure 1

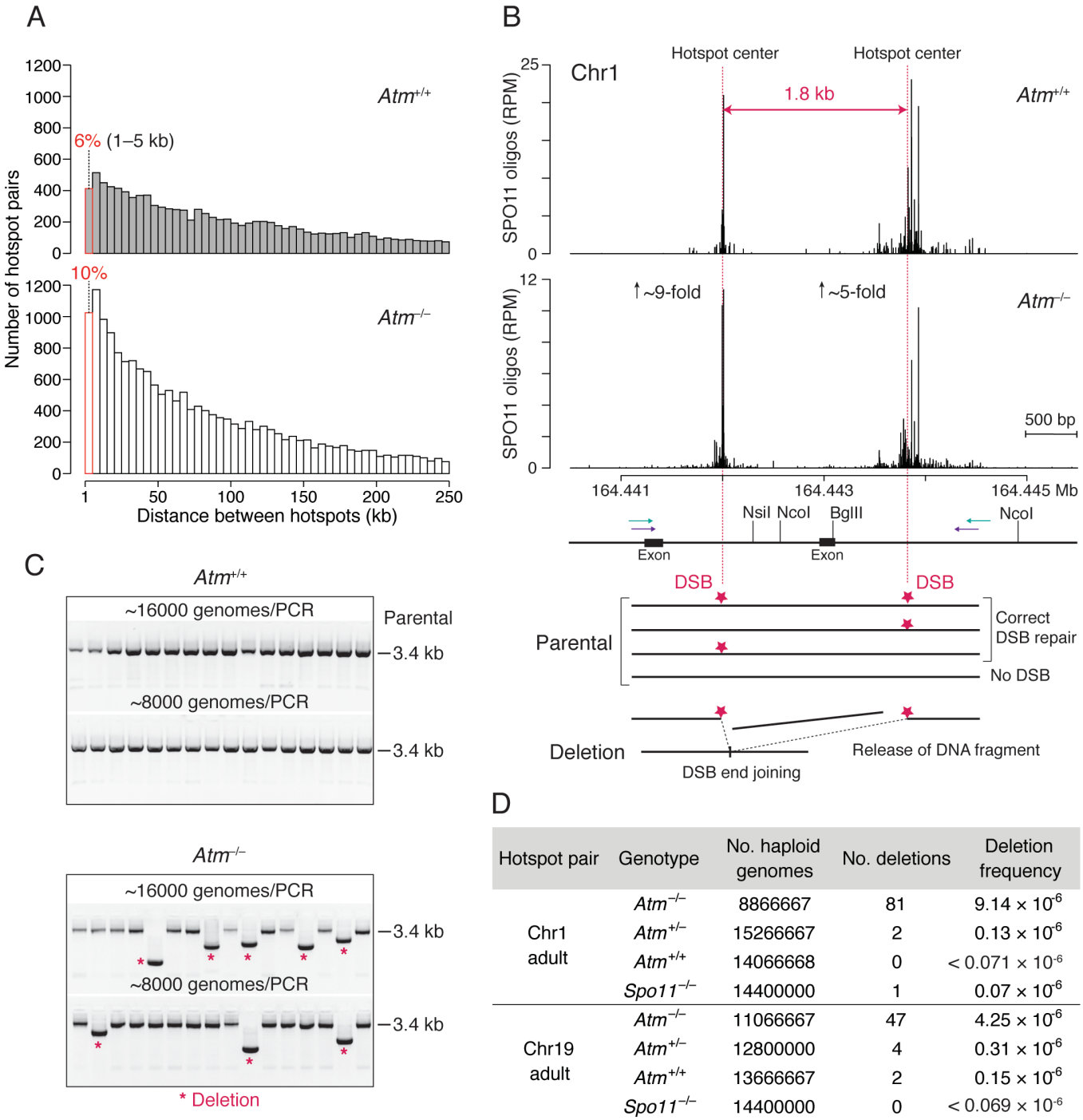

Hotspot pair	Genotype	No. haploid genomes	No. deletions	Deletion frequency
Chr1 adult	*Atm*$^{-/-}$	8866667	81	9.14×10^{-6}
	Atm$^{+/-}$	15266667	2	0.13×10^{-6}
	Atm$^{+/+}$	14066668	0	$< 0.071 \times 10^{-6}$
	Spo11$^{-/-}$	14400000	1	0.07×10^{-6}
Chr19 adult	*Atm*$^{-/-}$	11066667	47	4.25×10^{-6}
	Atm$^{+/-}$	12800000	4	0.31×10^{-6}
	Atm$^{+/+}$	13666667	2	0.15×10^{-6}
	Spo11$^{-/-}$	14400000	0	$< 0.069 \times 10^{-6}$

Figure 1. Meiotic deletions at adjacent DSB hotspots.
(A) Distribution of distances separating adjacent SPO11-oligo hotspots on autosomes. The hotspot calling algorithm[9] merges hotspots separated by edge-to-edge distances of <1 kb. Hotspot pairs separated by >250 kb are not shown. See also **Fig. S1**.

(B) Strategy to detect deletions between adjacent hotspots. Top panel, SPO11-oligo maps for the hotspot pair on Chr1 (RPM, reads per million). Genomic coordinates (MM10 assembly) are shown below the graphs. The estimated fold increase in absolute SPO11-oligo frequency (RPM × 11.3) is indicated for each hotspot. Vertical pink lines indicate hotspot centers. Lower panel, scheme of the PCR assay. Nested PCR across the DSB hotspot pair is carried out with the indicated primer pairs (arrows). Prior to amplification, genomic DNA is optionally digested with restriction enzymes to reduce amplification of parental products. The *Atp1b1* exon located between the two hotspots is removed in deletions.
(C) Detection of deletions by agarose gel electrophoresis. Representative gels for the Chr1 hotspot pair are shown. Each lane is a PCR seeded with the indicated number of haploid genomes.
(D) Deletion frequencies. Three to seven mice of each genotype per hotspot pair were analyzed, listed in **Table S1**.

Figure 2

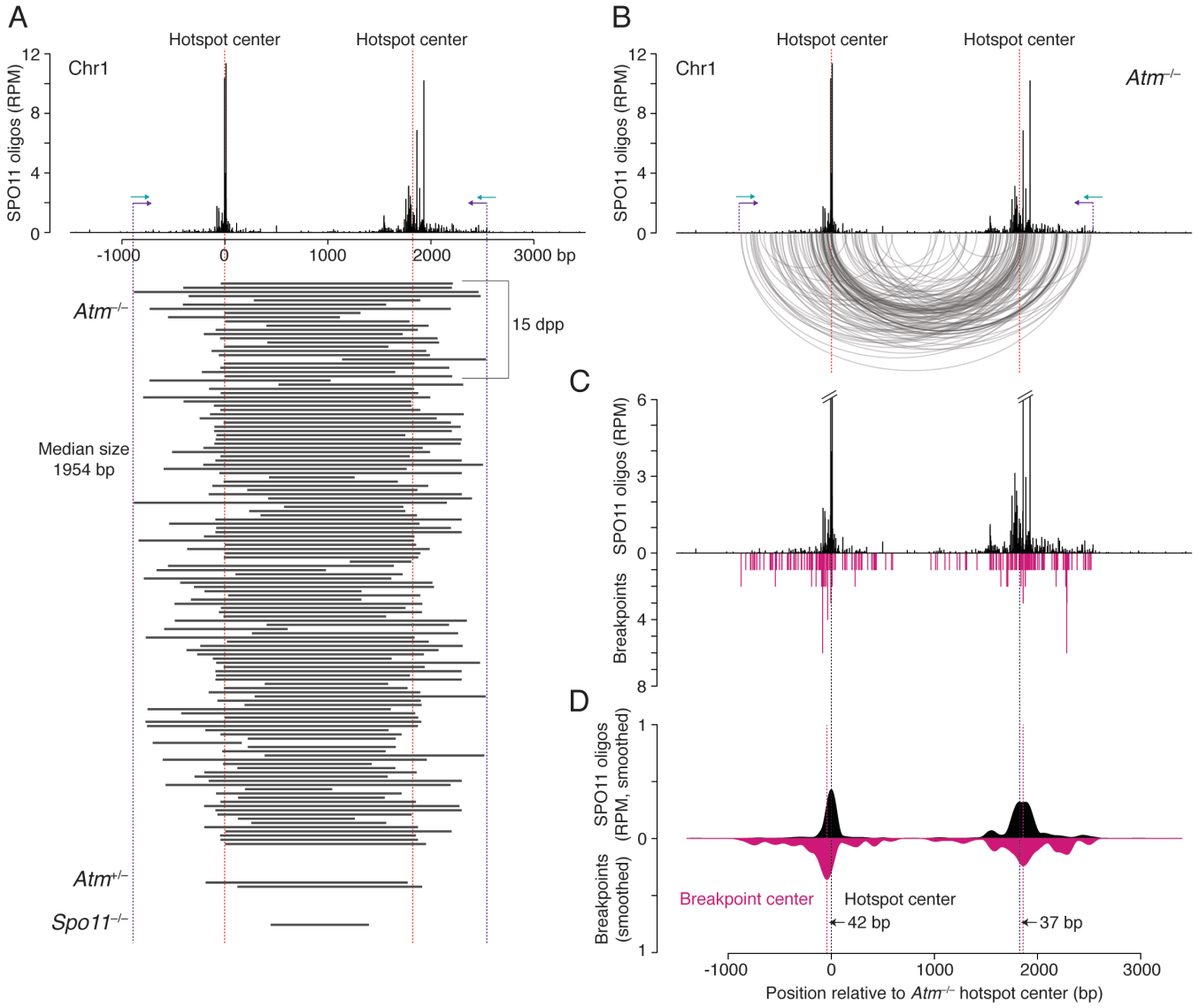

Figure 2. Deletion breakpoints at the Chr1 hotspot pair.
(A) Deleted DNA sequences at the Chr1 hotspot pair. Deletions (black bars) were combined from adult and juvenile testes (dpp, days post partum).
(B) Arc diagram of deletions in *Atm*$^{-/-}$ at the Chr1 hotspot pair. Arcs link the breakpoints of each deletion (134 deletions total). Both deletion breakpoints often mapped close to the hotspot centers. See also **Fig. S3**.
(C) Individual breakpoints cluster around the hotspot centers but are also observed to spread.
(D) Smoothed breakpoint and SPO11-oligo profiles display similar shapes (201-bp Hann filter for smoothing). Offsets between centers of hotspots and breakpoint distributions are indicated.

Figure 3

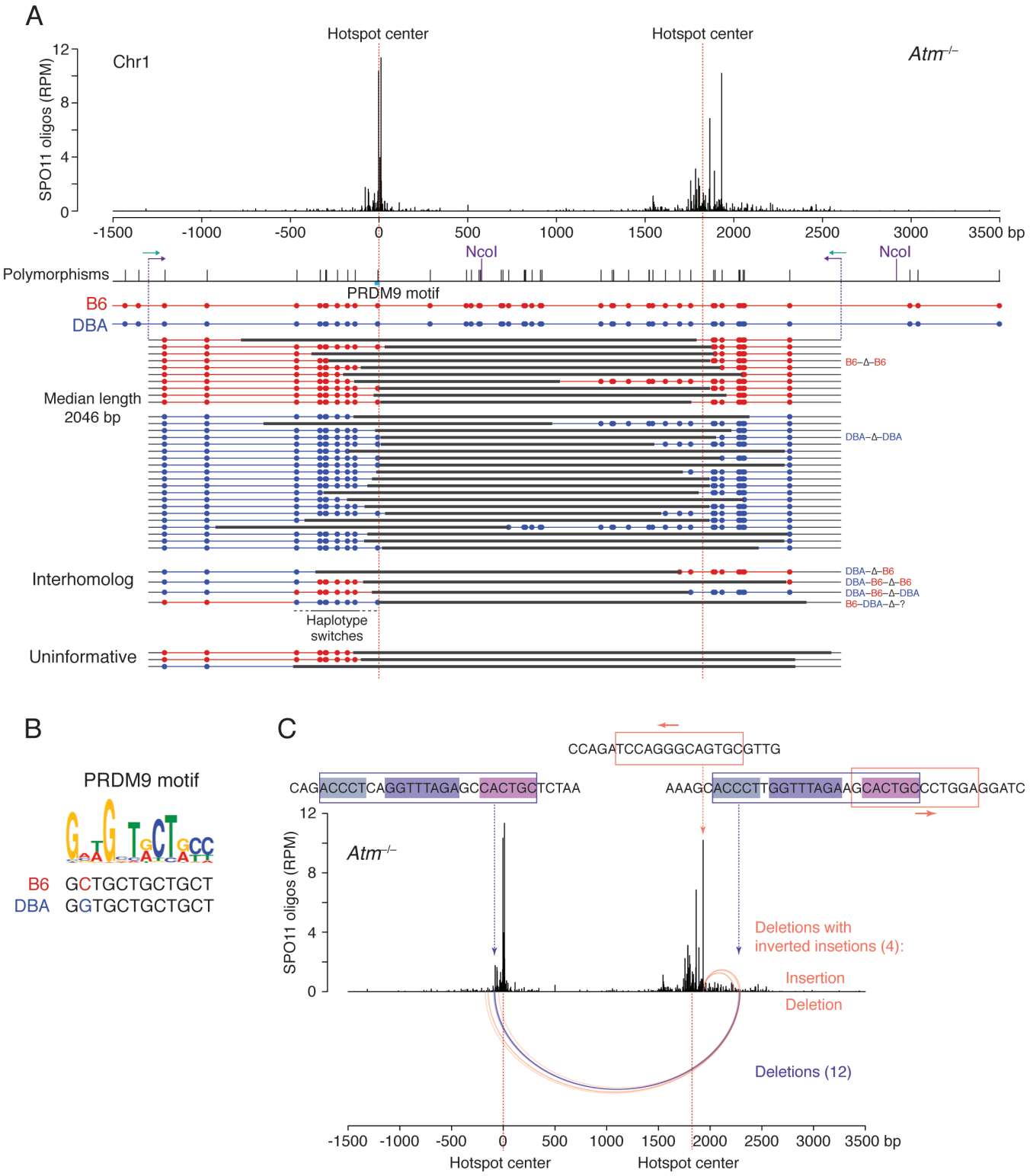
A
Hotspot center
Hotspot center
Chr1
Atm−/−
SPO11 oligos (RPM)
12
8
4
0
-1500
-1000
-500
0
500
1000
1500
2000
2500
3000
3500 bp
NcoI
NcoI
Polymorphisms
PRDM9 motif
B6
DBA
B6–Δ–B6
Median length
2046 bp
DBA–Δ–DBA
Interhomolog
DBA–Δ–B6
DBA–B6–Δ–B6
DBA–B6–Δ–DBA
B6–DBA–Δ–?
Haplotype
switches
Uninformative
B
PRDM9 motif
B6 GCTGCTGCTGCT
DBA GGTGCTGCTGCT
C
CCAGATCCAGGGCAGTGCGTTG
CAGACCCTCAGGTTTAGAGCCACTGCTCTAA
AAAGCACCCTTGGTTTAGAAGCACTGCCCTGGAGGATC
Atm−/−
SPO11 oligos (RPM)
Deletions with
inverted insetions (4):
Insertion
Deletion
Deletions (12)
Hotspot center
Hotspot center

Figure 3. Meiotic deletions within and between chromosomes.
(A) Deletions at the Chr1 hotspot pair in *Atm*$^{-/-}$ B6 × DBA F1 hybrid males. Nested PCR was performed with the indicated primers (arrows) to identify polymorphisms within the deletion products derived from B6 (red) or DBA (blue). Three deletions were uninformative because the involved chromosome(s) is uncertain.
(B) Predicted PRDM9 recognition sequences at the left hotspot in B6 and DBA, aligned to the PRDM9 motif from SPO11-oligo analysis[9].
(C) Recurrent deletion within the Chr1 hotspot pair at an imperfect repeat. Twelve simple deletions in *Atm*$^{-/-}$ map to this repeat at one of the three internal identical repeats of 5, 8, and 6 bp (violet arcs). Four other deletions with inverted insertions also involve this imperfect repeat as well as a 13-bp inverted microhomology at the hotspot center, with the insertions indicated above the deletions (orange arcs). See also **Fig. S7A, S9B**.

Figure 4

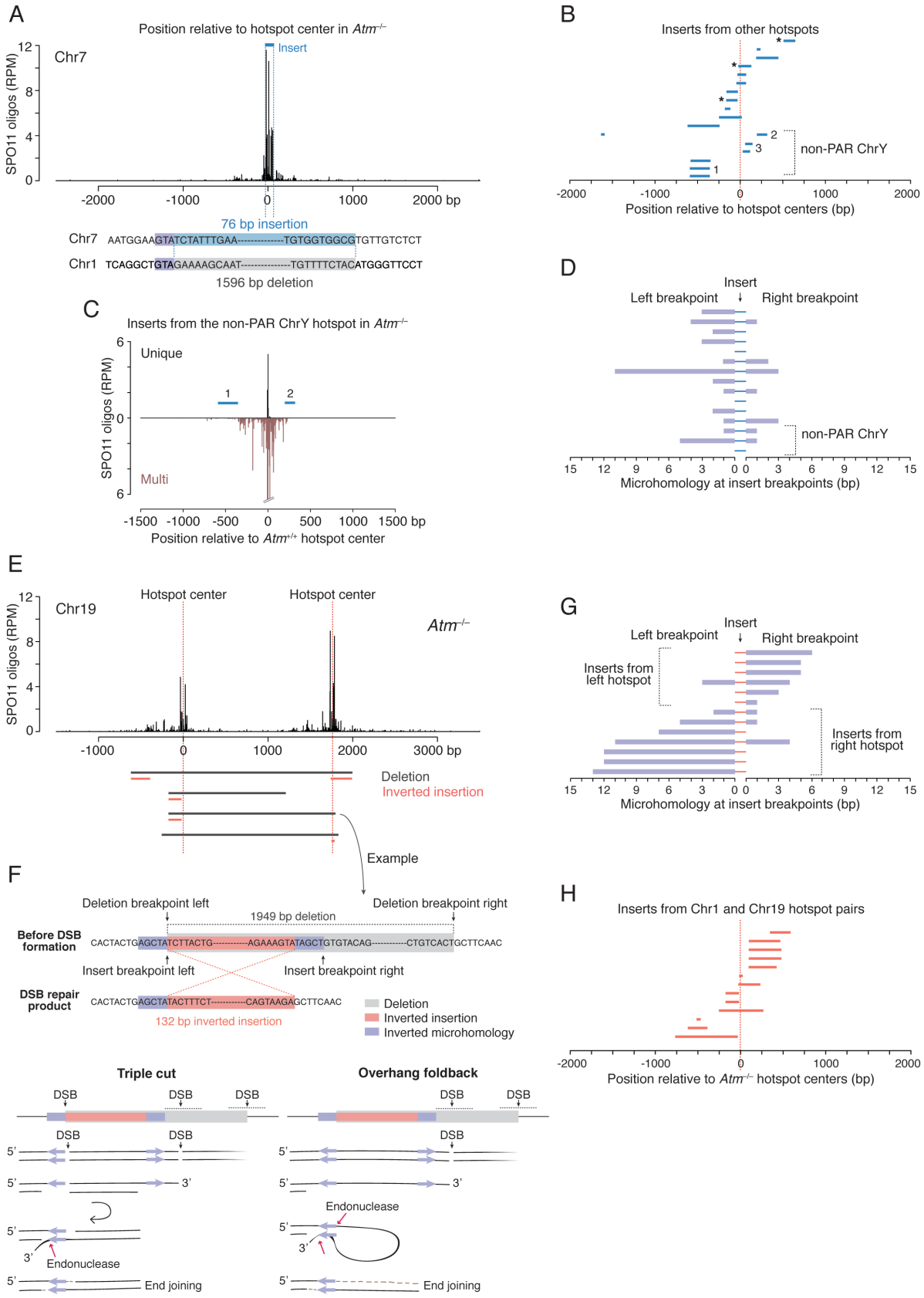
A
Position relative to hotspot center in Atm−/−
Chr7
Insert
SPO11 oligos (RPM)
-2000 -1000 0 1000 2000 bp
76 bp insertion
Chr7 AATGGAAGTATCTATTTGAA----------TGTGGTGGCGTGTTGTCTCT
Chr1 TCAGGCTGTAGAAAAGCAAT----------TGTTTTCTACATGGGTTCCT
1596 bp deletion
B
Inserts from other hotspots
non-PAR ChrY
Position relative to hotspot centers (bp)
C
Inserts from the non-PAR ChrY hotspot in Atm−/−
Unique
Multi
SPO11 oligos (RPM)
-1500 -1000 -500 0 500 1000 1500 bp
Position relative to Atm+/+ hotspot center
D
Insert
Left breakpoint
Right breakpoint
non-PAR ChrY
Microhomology at insert breakpoints (bp)
E
Chr19
Hotspot center
Hotspot center
Atm−/−
SPO11 oligos (RPM)
-1000 0 1000 2000 3000 bp
Deletion
Inverted insertion
Example
F
Deletion breakpoint left
Deletion breakpoint right
1949 bp deletion
Before DSB formation
CACTACTGAGCTATCTTACTG----------AGAAAGTATAGCTGTGTACAG----------CTGTCACTGCTTCAAC
Insert breakpoint left
Insert breakpoint right
DSB repair product
CACTACTGAGCTATACTTTCT----------CAGTAAGAGCTTCAAC
132 bp inverted insertion
Deletion
Inverted insertion
Inverted microhomology
Triple cut
Overhang foldback
DSB
5'
3'
Endonuclease
End joining
G
Insert
Left breakpoint
Right breakpoint
Inserts from left hotspot
Inserts from right hotspot
Microhomology at insert breakpoints (bp)
H
Inserts from Chr1 and Chr19 hotspot pairs
Position relative to Atm−/− hotspot centers (bp)

Figure 4. Insertions derived from DSB hotspots.
(A–D) Ectopic insertions from other hotspots. **A**, Example of a deletion on Chr1 from *Atm*$^{-/-}$ containing a 79-bp insertion derived from a hotspot on Chr7. **B**, Inserts from other hotspots map close to their respective hotspot centers. Three inserts map to SPO11-oligo clusters rather than called hotspots (asterisks). Inserts 1 and 3 from the non-PAR ChrY map to multiple hotspots. See also **Fig. S8, S10** and **Table S3**. **C**, Non-PAR ChrY hotspot to which inserts 1 and 2 can be mapped. Some SPO11 oligos can be uniquely mapped to this hotspot, but, as it is one copy of a family of repeats, numerous other SPO11 oligos can be mapped to both this and other copies of the repeat ("Multi"). **D**, Microhomologies at insert breakpoints are often short (median, 1 bp).
(E–H) Inverted insertions derived locally from the hotspot pair. **E**, Deletions with inverted insertions at the Chr19 hotspot pair. Inserts are derived in inverted orientation from the left or the right hotspot. For the Chr1 hotspot pair, see **Fig. S9B**. **F**, Example of an inverted insertion (top) and possible mechanisms (bottom). The right insertion breakpoint shares a 5-bp inverted microhomology with the left deletion breakpoint, while the left insertion breakpoint and the right deletion breakpoint do not share microhomology. Potential models explaining the inversion mechanism involve double cutting at the left hotspot or overhang foldback. **G**, Microhomologies at breakpoints for insertions derived from the Chr1 and Chr19 hotspot pairs. Inserts mapping to the left hotspot in a pair have long microhomologies present at their right breakpoints. Inserts mapping to the right hotspot mirror this pattern. See also **Table S4**. **H**, Inserts from the Chr1 and Chr19 hotspot pairs map close to hotspot centers.

Figure 5

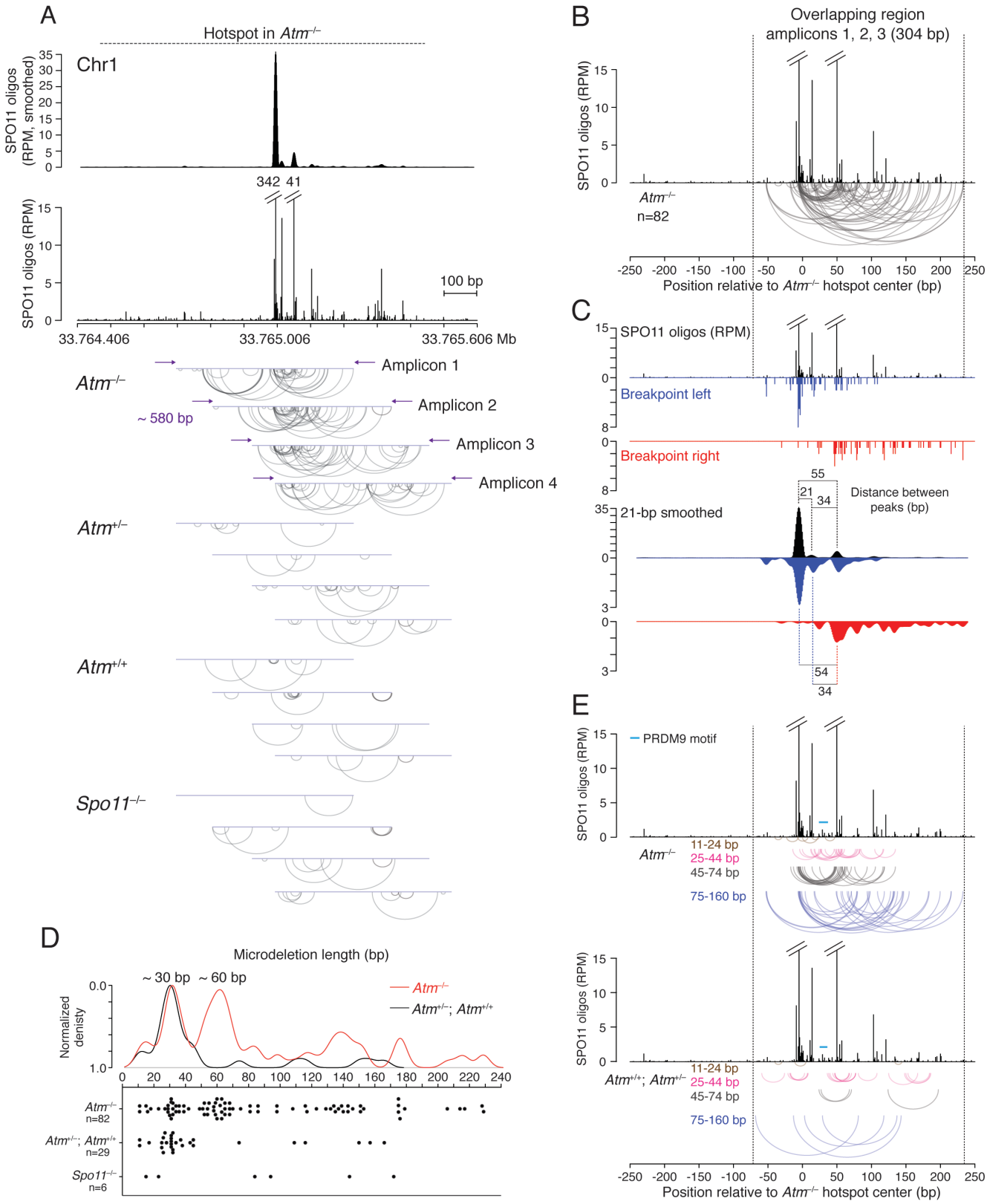
A
Hotspot in Atm−/−
Chr1
SPO11 oligos (RPM, smoothed)
342 41
SPO11 oligos (RPM)
100 bp
33.764.406
33.765.006
33.765.606 Mb
Atm−/−
Amplicon 1
Amplicon 2
~ 580 bp
Amplicon 3
Amplicon 4
Atm+/−
Atm+/+
Spo11−/−
B
Overlapping region
amplicons 1, 2, 3 (304 bp)
SPO11 oligos (RPM)
Atm−/−
n=82
Position relative to Atm−/− hotspot center (bp)
C
SPO11 oligos (RPM)
Breakpoint left
Breakpoint right
55
21
34
Distance between peaks (bp)
21-bp smoothed
54
34
D
Microdeletion length (bp)
~ 30 bp
~ 60 bp
Normalized denisty
Atm−/−
Atm+/−; Atm+/+
n=82
n=29
Spo11−/−
n=6
E
PRDM9 motif
SPO11 oligos (RPM)
Atm−/−
11-24 bp
25-44 bp
45-74 bp
75-160 bp
Atm+/+; Atm+/−
Position relative to Atm−/− hotspot center (bp)

Figure 5. Microdeletions within a single DSB hotspot.
(A) Detection of microdeletions at a strong DSB hotspot on Chr1 using amplicon deep sequencing. The hotspot displays a major SPO11-oligo peak, a secondary peak, and several minor peaks, as shown in the smoothed (21-bp Hann filter) and unsmoothed profiles. Four overlapping amplicons were deep sequenced to identify microdeletions. Arc diagrams of independent microdeletions found in each amplicon for the indicated genotypes are shown. For microdeletion frequencies, see **Table S5**.
(B, C) Microdeletions from *Atm*$^{-/-}$ in the region overlapping in amplicons 1, 2, and 3. **B**, Arc diagram of independent microdeletions. **C**, Distributions of the left and right breakpoints relative to the SPO11-oligo distribution. Both unsmoothed and smoothed profiles are shown.
(D, E) Microdeletion length distributions in the overlapping region. **D,** Density and scatter plots of microdeletion lengths (>10 bp). **E,** Arc diagrams of microdeletions stratified by length. Microdeletions >160 bp are not shown, as their location may be more restricted by the size of the assessed region. See also **Fig. S12B,C** for larger microdeletion distribution.

Figure S1

A

Dataset	No. hotspots	Hotspot pairs	No. hotspot pairs separated by 1-5 kb	Hotspots in hotspot pairs (%)
Atm$^{+/+}$	13436	*Atm*$^{+/+}$	413	6.1
Atm$^{-/-}$	20417	*Atm*$^{-/-}$	1023	10.0
shared	12172	both shared	304	3.0
new	8245	both new	241	2.4
		new+shared	478	4.7

B

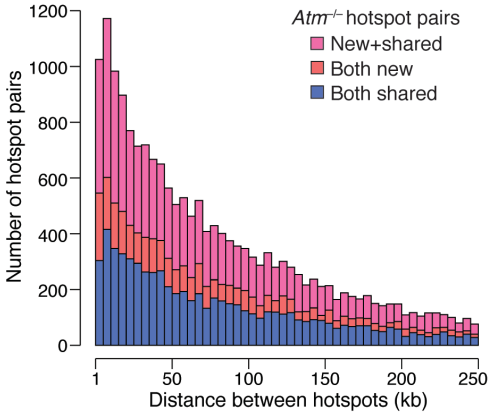

C

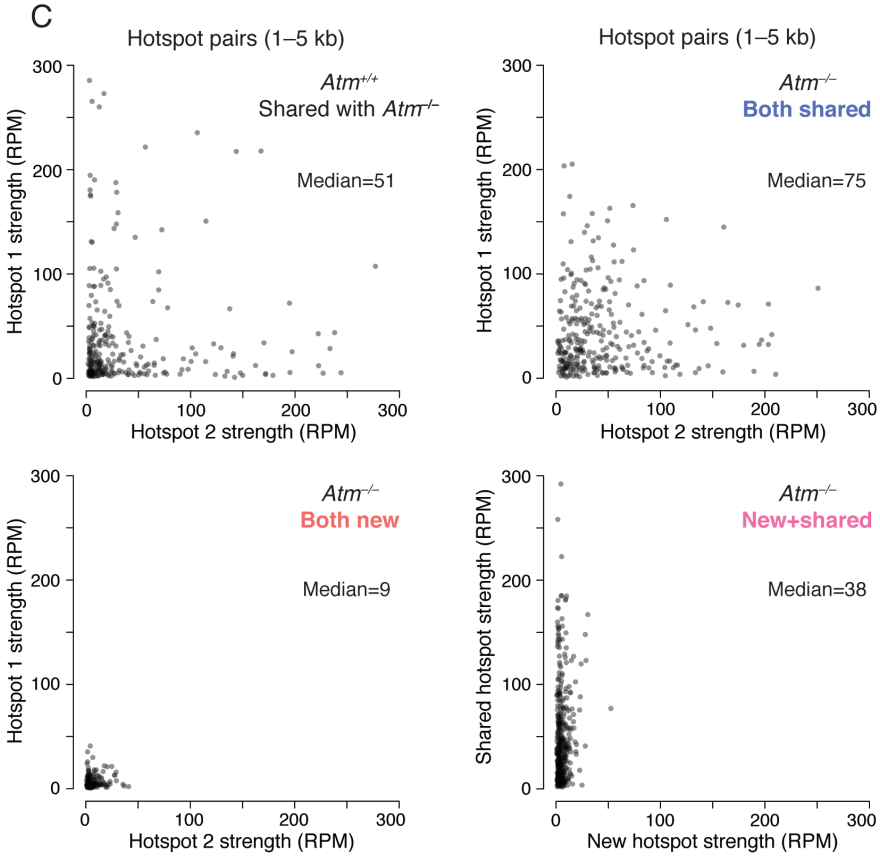

D

	Hotspot strength (RPM) [hotspot rank]		Fold increase in *Atm*$^{-/-}$ hotspot strength*
Chr1 pair	*Atm*$^{+/+}$	*Atm*$^{-/-}$	
hotspot left	65 [16%]	53 [16%]	9.2
hotspot right	209 [3%]	93 [6%]	5.0
Chr19 pair			
hotspot left	50 [20%]	41 [21%]	9.3
hotspot right	80 [13%]	69 [11%]	9.7

**Atm*$^{-/-}$ RPM divided by *Atm*$^{+/+}$ RPM multiplied by 11.3, the average increase in SPO11 oligos in *Atm*$^{-/-}$.

Figure S1. Higher potential in *Atm*$^{-/-}$ for DSB formation at adjacent hotspots.
Analyses were performed for autosomes.
(A) Hotspot pairs separated by 1–5 kb are observed more frequently in *Atm*$^{-/-}$ than in *Atm*$^{+/+}$. Data are derived from SPO11-oligo maps[9]. "Shared" hotspots are those called in both *Atm*$^{-/-}$ and *Atm*$^{+/+}$. "New" hotspots are those called only in *Atm*$^{-/-}$, although corresponding SPO11-oligo clusters are typically present in the *Atm*$^{+/+}$ map[9]. Hotspot pairs in *Atm*$^{-/-}$ are separated into classes according to whether each hotspot is shared or new.
(B) Distribution of distances separating hotspots in *Atm*$^{-/-}$ hotspot pairs, shown up to 250 kb. The proportion of each hotspot pair class from panel **A** is indicated. The increase in the number of hotspot pairs in *Atm*$^{-/-}$ separated by short distances (**Fig. 1A**) is primarily the result of the emergence of new hotspots close to shared hotspots.
(C) Strength of individual hotspots in hotspot pairs separated by 1–5 kb. Hotspot pair strength, the median of total RPM (reads per million) for the two hotspots in a pair, is indicated. Note that the RPM values do not account for the 11.3-fold increase in SPO11 oligos in *Atm*$^{-/-}$[4]. Outliers with >300 RPM (4 in *Atm*$^{-/-}$; 18 in *Atm*$^{+/+}$) are not shown.
(D) Hotspot strength for the individual hotspots in the Chr1 and Chr19 hotspot pairs. RPM values in *Atm*$^{-/-}$ are multiplied by 11.3, the average increase in whole-testis SPO11-oligo levels in *Atm*$^{-/-}$ mice. Hotspot rank is the rank of the individual hotspot within all hotspots for *Atm*$^{+/+}$ or *Atm*$^{-/-}$.

Figure S2

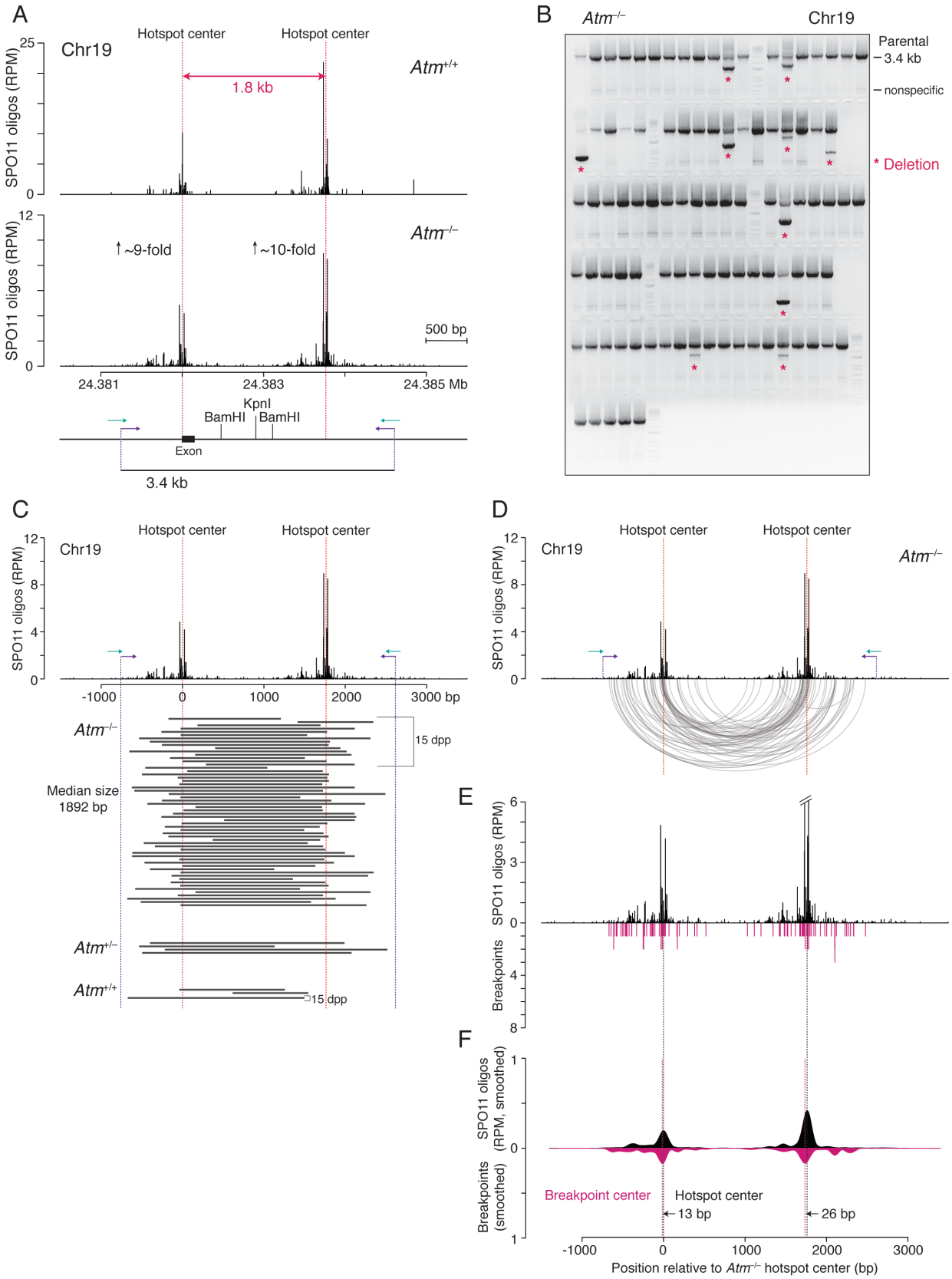
A
Chr19
Hotspot center
Hotspot center
1.8 kb
Atm+/+
SPO11 oligos (RPM)
25
0
12
0
↑~9-fold
↑~10-fold
Atm−/−
500 bp
24.381
24.383
24.385 Mb
KpnI
BamHI
BamHI
Exon
3.4 kb
B
Atm−/−
Chr19
Parental
3.4 kb
nonspecific
* Deletion
C
Chr19
Hotspot center
Hotspot center
SPO11 oligos (RPM)
12
8
4
0
-1000
0
1000
2000
3000 bp
Atm−/−
15 dpp
Median size
1892 bp
Atm+/−
Atm+/+
15 dpp
D
Chr19
Hotspot center
Hotspot center
Atm−/−
SPO11 oligos (RPM)
E
SPO11 oligos (RPM)
6
3
0
Breakpoints
4
8
F
SPO11 oligos (RPM, smoothed)
1
0
Breakpoints (smoothed)
1
Breakpoint center
Hotspot center
13 bp
26 bp
-1000
0
1000
2000
3000
Position relative to Atm−/− hotspot center (bp)

Figure S2. Deletions at the Chr19 hotspot pair.
(A) SPO11-oligo maps in wild type and *Atm*$^{-/-}$ at the Chr19 hotspot pair, with the scheme of the nested PCR assay below. The fold increase in the SPO11 oligos (RPM × 11.3) is indicated for each hotspot. Prior to amplification, genomic DNA is optionally digested with restriction enzymes to reduce amplification of parental products. The *Pip5k1b* exon located at the left hotspot is removed in many of the deletions.
(B) Representative gel of PCR products in *Atm*$^{-/-}$ from a 96-well plate. ~16,000 haploid genomes were seeded per PCR. Asterisks indicate deletions.
(C–F) Analysis of deletions. **C**, Deleted DNA sequences (black bars) from adult and juvenile testes. **D**, Arc diagram of deletions in *Atm*$^{-/-}$ (58 deletions total). See also **Fig. S3**. **E**, Distribution of individual breakpoints. **F**, Smoothed breakpoint and SPO11-oligo profiles (201-bp Hann filter for smoothing). Offsets between centers of hotspots and breakpoint distributions are indicated.

Figure S3

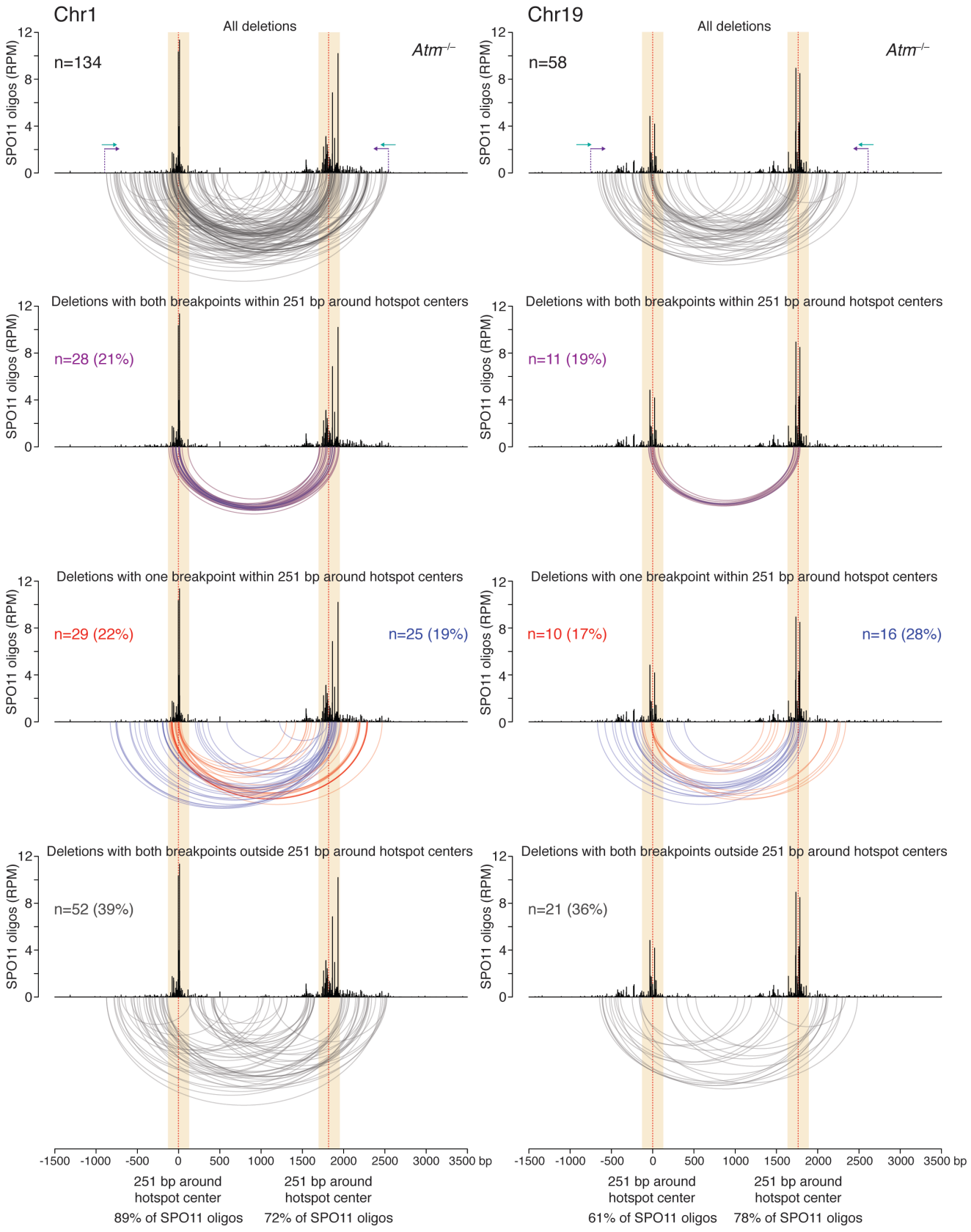
Chr1
All deletions
Atm-/-
n=134
Chr19
All deletions
Atm-/-
n=58
SPO11 oligos (RPM)
Deletions with both breakpoints within 251 bp around hotspot centers
n=28 (21%)
n=11 (19%)
Deletions with one breakpoint within 251 bp around hotspot centers
n=29 (22%)
n=25 (19%)
n=10 (17%)
n=16 (28%)
Deletions with both breakpoints outside 251 bp around hotspot centers
n=52 (39%)
n=21 (36%)
-1500 -1000 -500 0 500 1000 1500 2000 2500 3000 3500 bp
251 bp around hotspot center
89% of SPO11 oligos
72% of SPO11 oligos
61% of SPO11 oligos
78% of SPO11 oligos

Figure S3. Distribution of deletions for the Chr1 and Chr19 hotspot pairs.
Deletion arcs from *Atm*$^{-/-}$ are segregated according to the positions of breakpoints relative to 251-bp zones around each hotspot center (yellow). The percentage of SPO11 oligos shown at bottom is the number of SPO11 oligos within each 251-bp zone divided by the total number of SPO11 oligos mapping between the left or right primer (arrows) and the midpoint between hotspot centers. Deletions often have one (red and blue arcs) or both breakpoints (violet arcs) within the 251-bp zones.

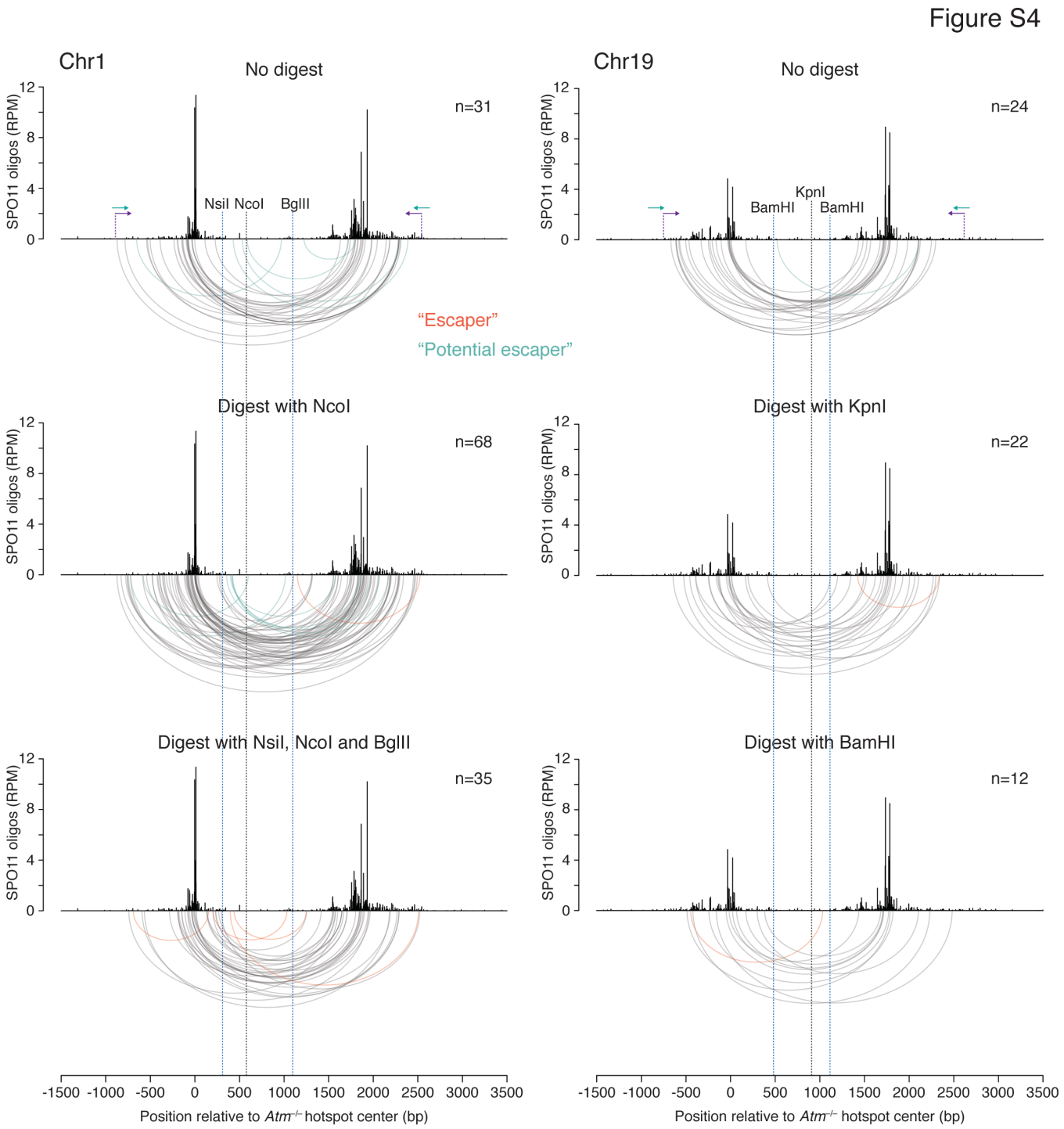

Figure S4. Distribution of deletions from experiments with or without prior genomic DNA digest. Genomic DNA was optionally digested with restriction enzymes prior to PCR to suppress amplification of parental DNA. Nested primers are indicated with arrows. Restriction sites located in between the two hotspots of a pair are expected to be absent in deletion products. Consistent with this, the majority of deletions in *Atm*$^{-/-}$ at the Chr1 and Chr19 hotspot pairs had both breakpoints outside of the restriction site region (vertical blue lines). Similar results were obtained in experiments in which the digestion step was

omitted, or only the enzyme cutting uniquely inside this region was used (NcoI or KpnI, vertical black lines). A few deletion products contained restriction sites due to incomplete genomic DNA digestion ("Escapers", orange arcs) or were captured in experiments with no digest or when the unique central cutting enzyme was used ("Potential escapers", green arcs). Overall, deletion distributions were similar in all experiments, independent of the digest, with breakpoints clustered around hotspot centers. Note that some of these deletions had both breakpoints mapping to one hotspot of the hotspot pair (4 at the Chr1 pair; 1 at the Chr19 pair), likely arising from DSBs formed within one hotspot, as with microdeletions.

Figure S5

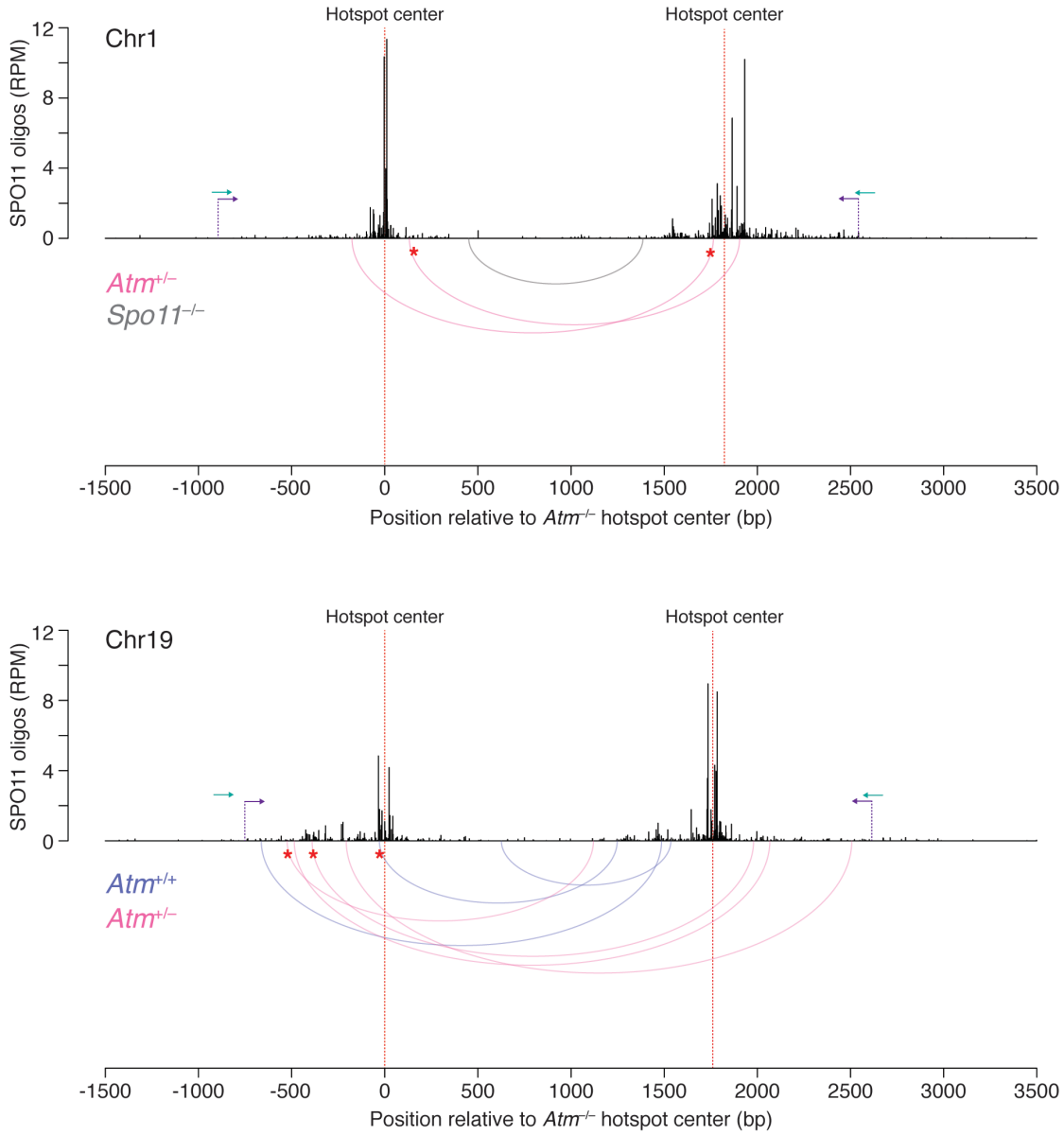

Figure S5. Deletions detected in the presence of ATM.
Deletions detected in *Atm*$^{+/+}$ (blue arcs) and *Atm*$^{+/-}$ (pink arcs) often had one breakpoint that was also found for a deletion in *Atm*$^{-/-}$ (red asterisks). The single deletion obtained from *Spo11*$^{-/-}$ at the Chr1 hotspot pair is also shown (grey arc).

Figure S6

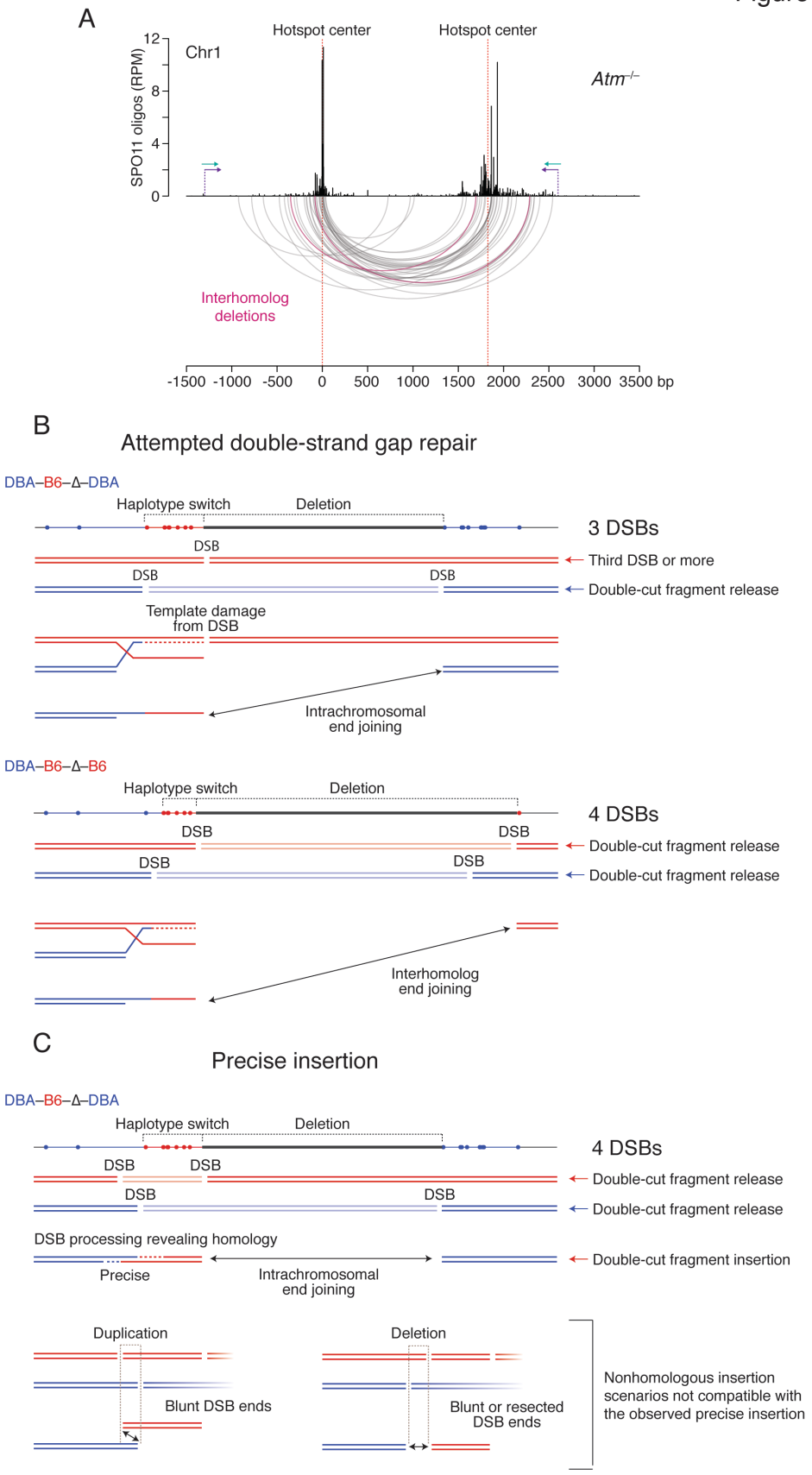
A
Hotspot center
Hotspot center
Chr1
Atm−/−
SPO11 oligos (RPM)
12
8
4
0
Interhomolog deletions
-1500 -1000 -500 0 500 1000 1500 2000 2500 3000 3500 bp
B
Attempted double-strand gap repair
DBA–B6–Δ–DBA
Haplotype switch
Deletion
3 DSBs
DSB
Third DSB or more
DSB
DSB
Double-cut fragment release
Template damage from DSB
Intrachromosomal end joining
DBA–B6–Δ–B6
Haplotype switch
Deletion
4 DSBs
DSB
DSB
Double-cut fragment release
DSB
DSB
Double-cut fragment release
Interhomolog end joining
C
Precise insertion
DBA–B6–Δ–DBA
Haplotype switch
Deletion
4 DSBs
DSB
DSB
Double-cut fragment release
DSB
DSB
Double-cut fragment release
DSB processing revealing homology
Double-cut fragment insertion
Precise
Intrachromosomal end joining
Duplication
Blunt DSB ends
Deletion
Blunt or resected DSB ends
Nonhomologous insertion scenarios not compatible with the observed precise insertion

Figure S6. Deletions in *Atm*$^{-/-}$ B6 × DBA F1 hybrid mice with models for haplotype switching.
(A) Arc diagram of deletions from the Chr1 hotspot pair (37 deletions total). Two interhomolog deletions are indicated (pink arcs).
(B, C). Models for haplotype switching in deletions. **B**, Attempted double-strand gap repair. Examples of one intrachromosomal (top) and one interhomolog (bottom) deletion with haplotype switches. In both cases, two DSBs produce a double-stranded gap between the two hotspots, releasing a double-cut fragment (lighter blue or red double line). One DSB end at the gap invades the homolog and is extended by DNA synthesis, but a DSB in the repair template leads to aborted synthesis, such that this end is ejected and joins the other end of the gap (intrachromosomal end joining) or the end of a DSB formed at the other hotspot in the homolog (interhomolog end joining). In the case of interhomolog deletions, it is also possible that only one DSB is formed on the chromosome initiating strand invasion. Thus, in both examples at least three DSBs occur, indicating extensive damage to multiple chromatids at adjacent hotspots when ATM is absent. The substantial template damage in this scenario may favor nonhomologous end-joining mechanisms. **C**, Precise insertion due to homologous annealing. An example of an intrachromosomal deletion with a haplotype switch. At a minimum four DSBs are formed, involving double cutting within one hotspot on one chromosome and at both hotspots on the other chromosome. A released double-cut fragment from one hotspot is precisely inserted at the double-stranded gap in the homolog through annealing of homologous sequences exposed by resection. Importantly this scenario depends on the relative position of the two DSBs in chromosomes. If the relative position were switched (bottom right), resection would not expose homologous sequences. Nonhomologous insertion is not compatible because it would produce a small deletion (bottom right) or a small duplication (bottom left). As we do not observe these types of repair products in our deletions, we consider the attempted double-strand gap repair scenario more likely.

Figure S7

A

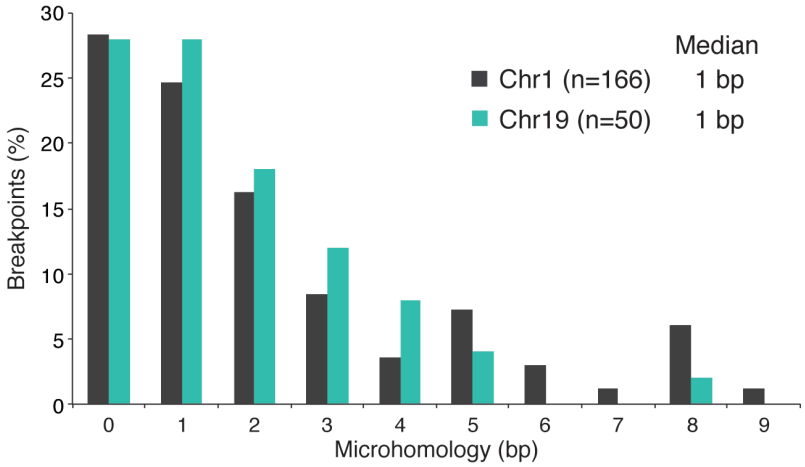

B

Recurring deletions on Chr1

Microhomology	Microhomology length (bp)	No. deletions	Deletion (bp)	Strain
–	0	2	1416	B6
CT	2	2	1868	B6, B6/DBA
AGCC	4	2	1943	B6, B6/DBA
ACCCT	5	2	2372	B6
AGACA	5	2	2816	B6, B6/DBA
CACTGC	6	2	2371	B6
GGTTTAGA	8	8	2371	B6 (6), B6/DBA (2)
AGCCAGTCA	9	2	1624	B6, B6/DBA
	median 6 bp			

Inverted microhomology	Microhomology length (bp)	No. deletions	Deletion/Insertion (bp)	Strain
CACTGCCCTGGA	12*	2	2437/356	B6
		24 of total 185 deletions		

Figure S7. Microhomology at deletion breakpoints in *Atm*$^{-/-}$.
(A) Distribution of microhomology lengths for the Chr1 and Chr19 hotspot pairs deletion breakpoints. Only deletions without insertions are included (**Table S2**).
(B) Recurring deletions at the Chr1 hotspot pair in B6 inbred and B6 × DBA F1 hybrid mice. Recurring deletions often had longer microhomologies at breakpoints. Microhomologies within the larger imperfect repeat described in the text are marked in different colors as in **Fig. 3C**. A recurring deletion with inverted insertion (asterisk) with a 12-bp microhomology at one insert breakpoint is also shown (**Fig. 3C, S9B**).

Figure S8

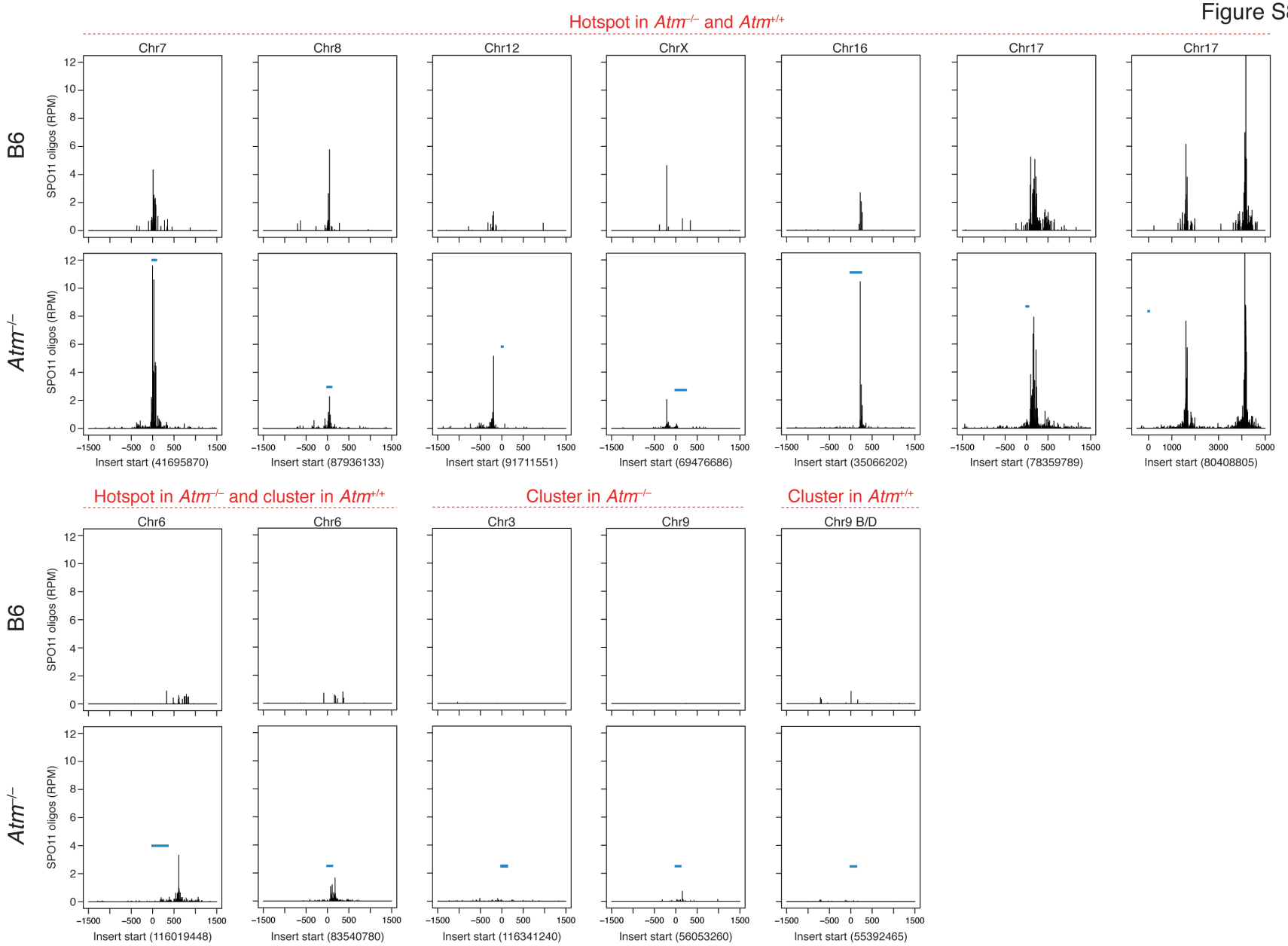
Hotspot in Atm−/− and Atm+/+
Chr7
Chr8
Chr12
ChrX
Chr16
Chr17
Chr17
B6
Atm−/−
SPO11 oligos (RPM)
Insert start (41695870)
Insert start (87936133)
Insert start (91711551)
Insert start (69476686)
Insert start (35066202)
Insert start (78359789)
Insert start (80408805)
Hotspot in Atm−/− and cluster in Atm+/+
Cluster in Atm−/−
Cluster in Atm+/+
Chr6
Chr6
Chr3
Chr9
Chr9 B/D
Insert start (116019448)
Insert start (83540780)
Insert start (116341240)
Insert start (56053260)
Insert start (55392465)

Figure S8. Derivation of inserts mapping to DSB hotspots on other chromosomes.
SPO11 oligos at the genomic locations of inserts (blue bars) are shown for *Atm*$^{-/-}$ and *Atm*$^{+/+}$ and indicated as to whether they were called as hotspots in one or both genotypes or instead contain SPO11-oligo clusters. Inserts mapping to the non-PAR ChrY are shown in **Fig. S10**. One insert mapping to a microsatellite repeat is not shown. See also **Table S3**.

Figure S9

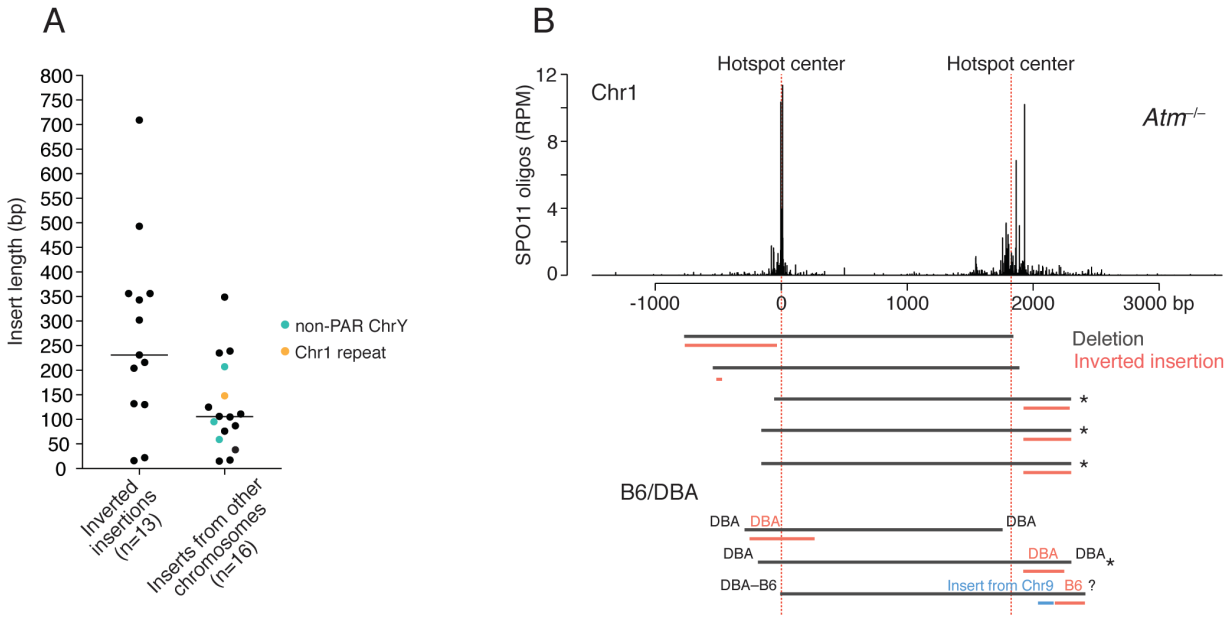

Figure S9. Characteristics of insertions in *Atm*$^{-/-}$.

(A) Inverted insertions from the same hotspot pair have a broader distribution of lengths than inserts derived from other chromosomes. Median insert lengths are indicated. See also **Tables S3, S4**.

(B) Deletions with inverted insertions at the Chr1 hotspot pair in B6 and B6 × DBA mice. Asterisks denote deletions where one insert breakpoint had the same microhomology as the site with recurring deletions (**Fig. 3C**). Note that for the two deletions on the DBA chromosome, the inserts also derived from the DBA chromosome.

Figure S10

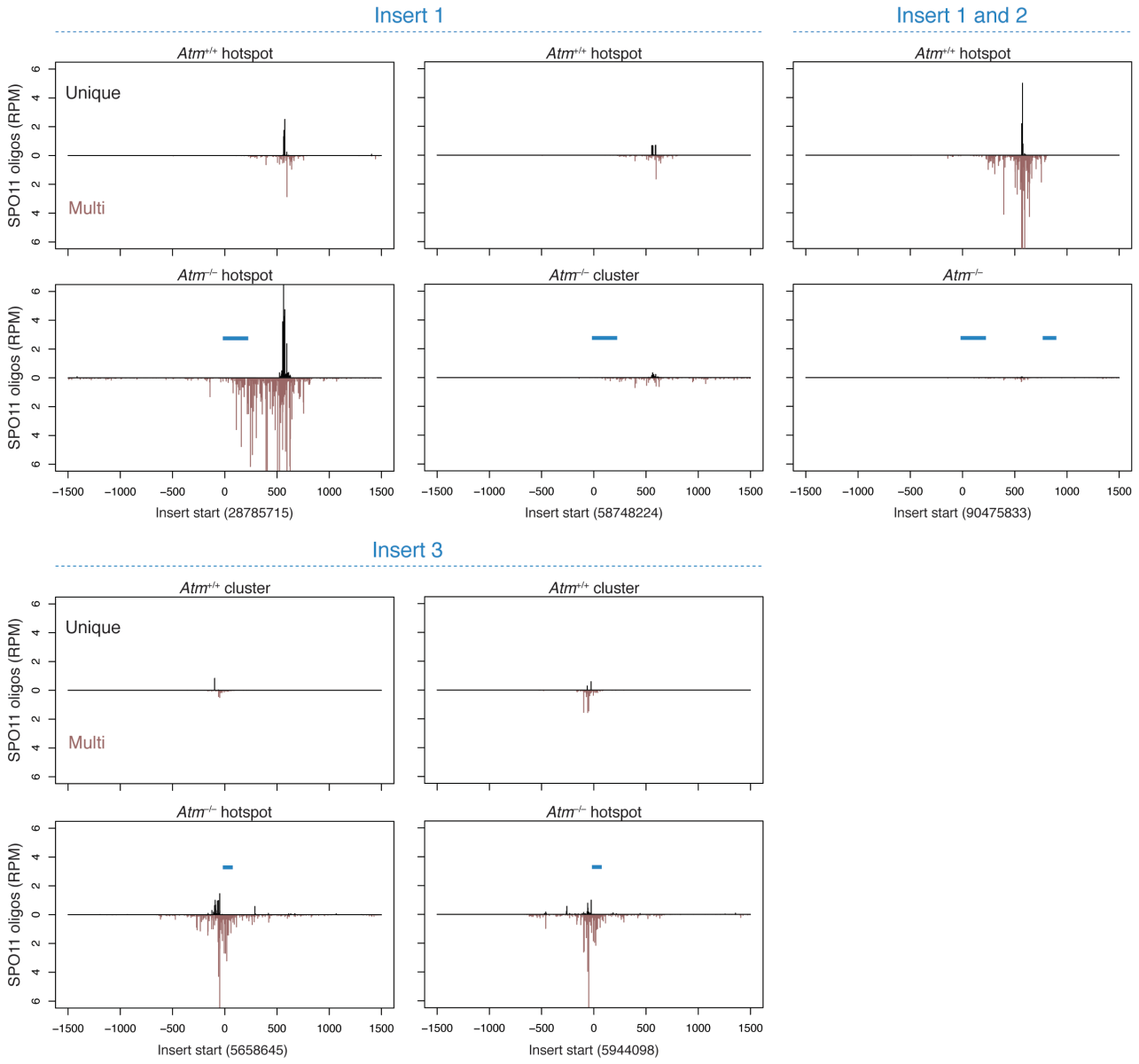

Figure S10. Inserts from the non-PAR ChrY map to multiple DSB hotspots.
Three inserts identified in *Atm*$^{-/-}$ deletions map to non-PAR ChrY repeats (**Table S3**), some of which have called hotspots. SPO11-oligo profiles are shown only for those repeats containing hotspots in *Atm*$^{-/-}$, *Atm*$^{+/+}$, or both, with the position of the inserts (blue bars) for each hotspot indicated. Inserts 1 and 2 are part of the same repeat family, and in one case they map to a single hotspot. Inserts 1 and 3 map to three and two hotspots, respectively. SPO11 oligos map uniquely to these hotspots ("Unique") or also map to other copies of the repeats ("Multi"). It remains possible that other repeat locations to which SPO11 oligos do not map uniquely also contain hotspots. Given that all insert-matching repeats (67 total) contain an intact PRDM9 motif, it is possible that DSBs are formed in many such repeats. The locations of multi-mapping SPO11 oligos were imputed, meaning they were distributed among mapped positions proportionally to local densities of uniquely mapping SPO11 oligos[9].

Figure S11

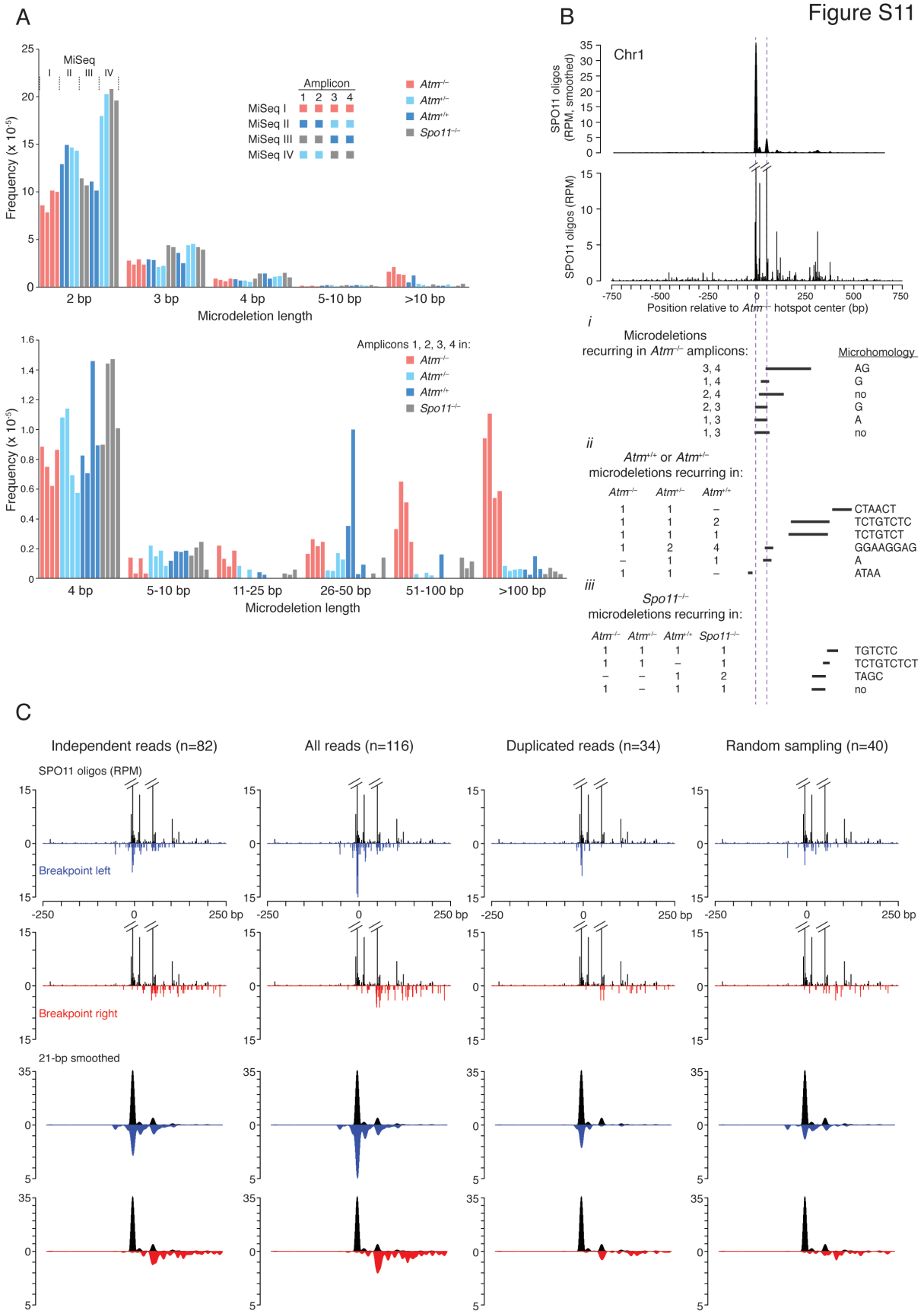
A
MiSeq
I
II
III
IV
Amplicon
1 2 3 4
MiSeq I
MiSeq II
MiSeq III
MiSeq IV
Atm−/−
Atm+/−
Atm+/+
Spo11−/−
Frequency (x 10-5)
2 bp
3 bp
4 bp
5-10 bp
>10 bp
Microdeletion length
Amplicons 1, 2, 3, 4 in:
4 bp
5-10 bp
11-25 bp
26-50 bp
51-100 bp
>100 bp
B
Chr1
SPO11 oligos (RPM, smoothed)
SPO11 oligos (RPM)
Position relative to Atm−/− hotspot center (bp)
i
Microdeletions recurring in Atm−/− amplicons:
Microhomology
3, 4 AG
1, 4 G
2, 4 no
2, 3 G
1, 3 A
1, 3 no
ii
Atm+/+ or Atm+/− microdeletions recurring in:
Atm−/− Atm+/− Atm+/+
1 1 –
1 1 2
1 1 1
1 2 4
– 1 1
1 1 –
CTAACT
TCTGTCTC
TCTGTCT
GGAAGGAG
A
ATAA
iii
Spo11−/− microdeletions recurring in:
Atm−/− Atm+/− Atm+/+ Spo11−/−
1 1 1 1
1 1 – 1
– – 1 2
1 – 1 1
TGTCTC
TCTGTCTCT
TAGC
no
C
Independent reads (n=82)
All reads (n=116)
Duplicated reads (n=34)
Random sampling (n=40)
SPO11 oligos (RPM)
Breakpoint left
Breakpoint right
21-bp smoothed
-250
0
250 bp

Figure S11. Evaluation of reads with microdeletions from deep sequencing of a single hotspot.
(A) Frequency of reads that had microdeletions of the indicated lengths. Four overlapping amplicons across the hotspot (1–4) were deep sequenced using MiSeq. For each amplicon, 576 separate PCRs were carried out with a total input of 9.6 million haploid genome equivalents, using a limited number of amplification cycles (see Methods). The PCR products for each amplicon were then pooled for sequencing. Four MiSeq runs were performed (I–IV) with the indicated amplicons and genotypes. For clarity, sequencing results are grouped by run (Top) or genotype (Bottom). At top, note that reads with small deletions (2–4 bp) were frequently observed in all amplicons for each genotype, including *Spo11*$^{-/-}$, and that their frequency varied between sequencing runs, indicating a significant batch effect. Short deletions (e.g., 2 bp) are known to arise from PCR and sequencing errors[63], and we saw that they became progressively less abundant in all genotypes up to 10 bp. Excluded from the 4-bp deletions is a product that was represented by >1000 reads in amplions 1–3. By contrast, reads with deletions >10 bp were more frequent in *Atm*$^{-/-}$ than in the other genotypes. At bottom, note that reads with 11–25-bp microdeletions were more frequent in *Atm*$^{-/-}$. Therefore, 11 bp was used as the lower cutoff to define a microdeletion for subsequent analyses. Our sequencing design (pooling of many low-cycle PCRs) is expected to minimize PCR jackpots and reduce instances where PCR duplicates from the same input DNA molecule are sequenced. However, two amplicons in *Atm*$^{+/+}$ showed multiple reads for one microdeletion each (amplicon 1: 26-bp microdeletion, 14 reads; amplicon 2: 31-bp microdeletion, 22 reads; **Table S5**), which therefore may be PCR duplicates. Thus, in some subsequent analyses we applied a stringent definition of independent events by including only one read for a given deletion product from a given amplicon.
(B) Recurring microdeletions within the hotspot. Top, smoothed (21-bp Hann filter) and unsmoothed SPO11-oligo maps at the Chr1 hotspot in *Atm*$^{-/-}$. Bottom, recurring microdeletions. These identical microdeletions (black bars) were found in independent PCRs for different amplicons. i) In *Atm*$^{-/-}$, amplicons that yielded the recurring microdeletions are indicated. For example, the microdeletion with the AG microhomology arose in amplicons 3 and 4. Note that one or both breakpoints for each of the recurring microdeletions occured at SPO11-oligo peaks (dashed vertical lines). ii) In *Atm*$^{+/-}$ and *Atm*$^{+/+}$, some microdeletions were identical to those found in *Atm*$^{-/-}$, in some cases in multiple amplicons. For example, the microdeletion with the GGAAGGAG microhomology was recovered in all three genotypes, but in different amplicons (*Atm*$^{-/-}$, 1; *Atm*$^{+/-}$, 2; *Atm*$^{+/+}$, 4). iii) Some of the microdeletions found in *Spo11*$^{-/-}$ recurred in other genotypes. Note that these map to the same region of the hotspot away from the center.
(C) Many of the duplicated reads in *Atm*$^{-/-}$ amplicons likely represent independent microdeletion events rather than PCR duplicates. For each amplicon, we randomly sampled with replacement from a set of reads representing all of the unique microdeletions observed. The sampled group was equal in number to the duplicated reads actually obtained for that amplicon. Then, the sampled reads with microdeletions mapping to the region where amplicons 1, 2, and 3 overlap were combined, and their breakpoint distribution was compared with the distribution of the observed duplicate reads. Breakpoint profiles of independently obtained reads, as in **Fig. 5C**, and of all reads are also shown. In the smoothed breakpoint profiles of the observed duplicates, the left breakpoints were particularly enriched in a peak that matched the central peak of SPO11 oligos, and the right breakpoints were enriched at a position that matched the secondary peak of SPO11 oligos. These patterns were not recapitulated by random sampling: both the left and right breakpoints were more widely dispersed without such clear enrichment coincident with the SPO11-oligo peaks. Because the observed duplicates were more likely than the random sample to have breakpoints aligned with the strongly favored locations of DSBs, these findings are consistent with the conclusion that most of the duplicated reads represent independent microdeletion events.

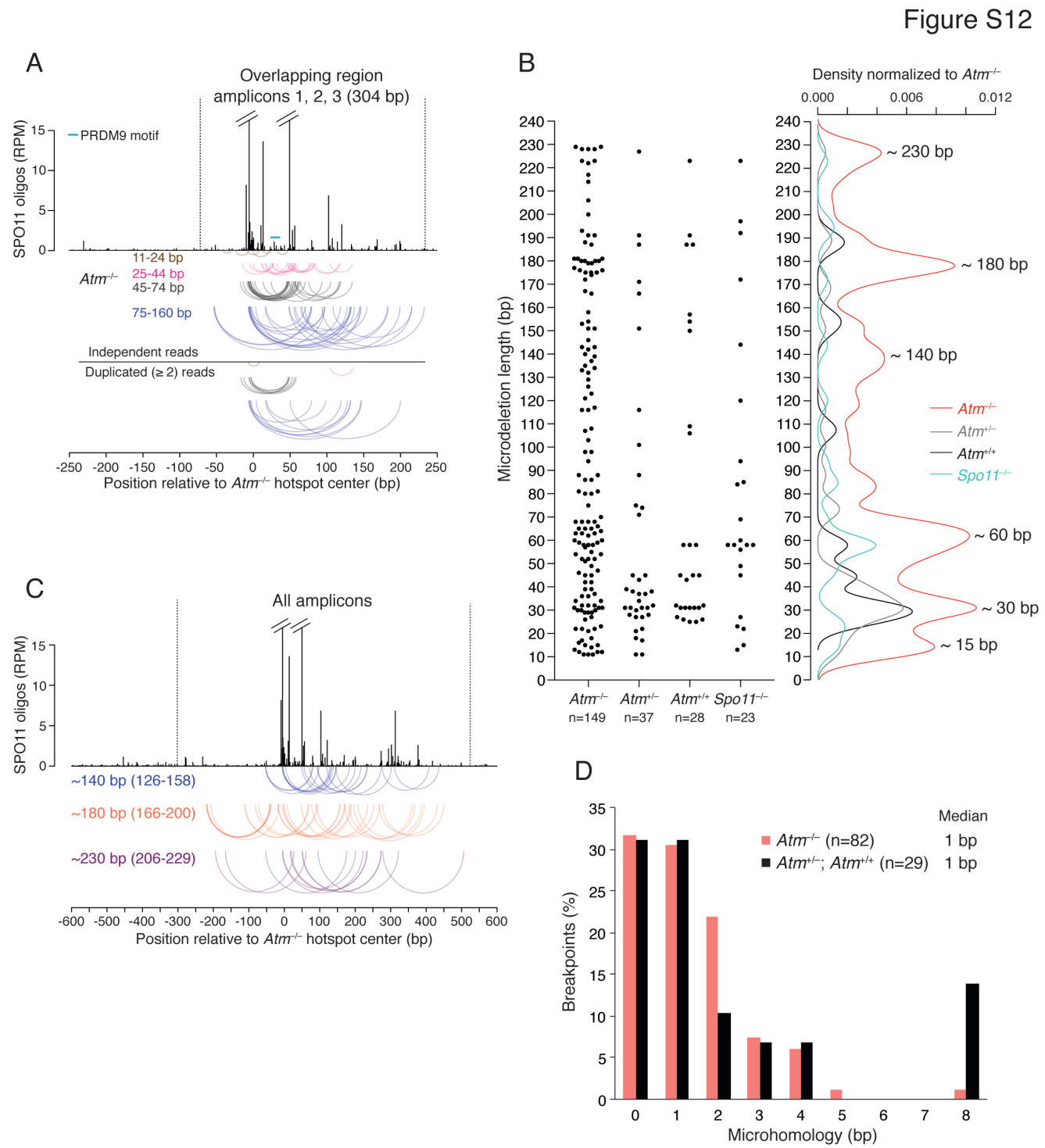

Figure S12. Extended analysis of microdeletions by genotype and microhomology.
(A) Arc diagrams of microdeletions stratified by length from *Atm*$^{-/-}$, as in **Fig. 5C**, with microdeletions in duplicated reads below. Microdeletions >160 bp are not shown, as their location may be more constrained by restricting analysis to the region where the amplicons overlap.

(B) Microdeletion length distribution for all amplicons by genotype for independent reads. Scatter plots and corresponding density plots are shown (>10 bp); densities in *Atm*$^{+/-}$, *Atm*$^{+/+}$, and *Spo11*$^{-/-}$ are normalized to *Atm*$^{-/-}$ to reflect read numbers in each genotype. As in the analysis of microdeletions in the overlap region of amplicons 1, 2, and 3 (**Fig. 5D**), distinct size classes were observed in the presence and absence of ATM, but not in *Spo11*$^{-/-}$. Larger microdeletion size classes (~140 bp, ~180 bp, ~230 bp) were well defined when all amplicons are considered. A smaller size class (~15 bp) was more prominent outside of the overlap region.
(C) Arc diagrams of the ~140-bp, ~180-bp, and ~230-bp microdeletions observed for *Atm*$^{-/-}$.
(D) Microhomology lengths at microdeletion breakpoints in the presence and absence of ATM. Analyses were performed for independent microdeletions in the overlapping region between amplicons 1, 2, and 3.

Table S1. Frequency of deletions in testis from individual mice.

Strain background	Hotspot pair	Mouse and genotype	No. haploid genomes	No. deletions	Frequency
B6	Chr1 adult	1794 *Atm*$^{-/-}$	5400000	67	12.41×10^{-6}
		*1793 *Atm*$^{+/+}$	5400000	0	$< 0.19 \times 10^{-6}$
		*2018 *Atm*$^{-/-}$	2066667	8	3.87×10^{-6}
		*2017 *Atm*$^{+/-}$	2066667	0	$< 0.48 \times 10^{-6}$
		*2066 *Atm*$^{+/-}$	1600000	0	$< 0.63 \times 10^{-6}$
		*2067 *Atm*$^{+/+}$	2266668	0	$< 0.44 \times 10^{-6}$
		*2656 *Atm*$^{-/-}$	1400000	6	4.29×10^{-6}
		*2657 *Atm*$^{+/-}$	3200000	0	$< 0.31 \times 10^{-6}$
		*2732 *Atm*$^{+/-}$	6400000	2	0.31×10^{-6}
		*2970 *Atm*$^{+/-}$	2000000	0	$< 0.50 \times 10^{-6}$
		*3162 *Atm*$^{+/+}$	6400000	0	$< 0.16 \times 10^{-6}$
		*3312 *Spo11*$^{-/-}$	6400000	0	$< 0.16 \times 10^{-6}$
		*3345 *Spo11*$^{-/-}$	6400000	0	$< 0.16 \times 10^{-6}$
		*3424 *Spo11*$^{-/-}$	1600000	1	0.63×10^{-6}
		Total *Atm*$^{-/-}$	8866667	81	9.14×10^{-6}
		Total *Atm*$^{+/-}$	15266667	2	0.13×10^{-6}
		Total *Atm*$^{+/+}$	14066668	0	$< 0.071 \times 10^{-6}$
		Total *Spo11*$^{-/-}$	14400000	1	0.07×10^{-6}
B6	Chr1 juvenile	*1 *Atm*$^{-/-}$	3200000	24	7.50×10^{-6}
		*2 *Atm*$^{+/-}$	3200000	0	$< 0.31 \times 10^{-6}$
		*3 *Atm*$^{+/+}$	3200000	0	$< 0.31 \times 10^{-6}$
F1 B6/DBA	Chr1 adult	2654 *Atm*$^{-/-}$	3600000	7	1.94×10^{-6}
		2675 *Atm*$^{-/-}$	5200000	30	5.77×10^{-6}
		2674 *Atm*$^{+/-}$	3200000	0	$< 0.31 \times 10^{-6}$
		2647 *Atm*$^{+/+}$	3200000	0	$< 0.31 \times 10^{-6}$
		Total *Atm*$^{-/-}$	8800000	37	4.20×10^{-6}
B6	Chr19 adult	*1793 *Atm*$^{+/+}$	5400000	2	0.37×10^{-6}
		*2018 *Atm*$^{-/-}$	266667	2	7.50×10^{-6}
		*2017 *Atm*$^{+/-}$	400000	0	$< 0.25 \times 10^{-5}$
		*2066 *Atm*$^{+/-}$	1600000	0	$< 0.63 \times 10^{-6}$
		*2067 *Atm*$^{+/+}$	1866667	0	$< 0.54 \times 10^{-6}$
		*2656 *Atm*$^{-/-}$	3200000	7	2.19×10^{-6}
		*2657 *Atm*$^{+/-}$	3200000	1	0.31×10^{-6}
		2733 *Atm*$^{-/-}$	4800000	29	6.04×10^{-6}
		*2732 *Atm*$^{+/-}$	4800000	3	0.63×10^{-6}
		2734 *Atm*$^{-/-}$	400000	2	5.00×10^{-6}
		2731 *Atm*$^{+/-}$	400000	0	$< 2.5 \times 10^{-6}$
		2780 *Atm*$^{-/-}$	400000	2	5.00×10^{-6}
		2779 *Atm*$^{+/-}$	400000	0	$< 2.5 \times 10^{-6}$
		2971 *Atm*$^{-/-}$	2000000	5	2.50×10^{-6}
		*2970 *Atm*$^{+/-}$	2000000	0	$< 0.50 \times 10^{-6}$
		*3162 *Atm*$^{+/+}$	6400000	0	$< 0.16 \times 10^{-6}$
		*3312 *Spo11*$^{-/-}$	6400000	0	$< 0.16 \times 10^{-6}$
		*3345 *Spo11*$^{-/-}$	6400000	0	$< 0.16 \times 10^{-6}$
		*3424 *Spo11*$^{-/-}$	1600000	0	$< 0.63 \times 10^{-6}$
		Total *Atm*$^{-/-}$	11066667	47	4.25×10^{-6}
		Total *Atm*$^{+/-}$	12800000	4	0.31×10^{-6}
		Total *Atm*$^{+/+}$	13666667	2	0.15×10^{-6}
		Total *Spo11*$^{-/-}$	14400000	0	$< 0.069 \times 10^{-6}$
B6	Chr19 juvenile	*1 *Atm*$^{-/-}$	1600000	11	6.88×10^{-6}
		*2 *Atm*$^{+/-}$	3200000	0	$< 0.31 \times 10^{-6}$
		*3 *Atm*$^{+/+}$	3200000	1	0.31×10^{-6}

Littermates are grouped. * The same mice used for both hotspot pairs.

Table S2. Deletions detected in *Atm*$^{-/-}$ with the analyses performed.

Hotspot pair	Strain background (primer set)[a]	No. PCR reactions	DNA (ng) seeded in PCR	No. haploid genomes	Total No. deletions	No. of deletions with insertions	Analyses performed
Chr1	B6 (b6)	168	25	1400000	16	0	frequency, breakpoint distribution, microhomology, insertions, recurring deletions
		640	50	10666667	89	12	frequency, breakpoint distribution, microhomology, insertions, recurring deletions
		72	100	2400000	29	3	breakpoint distribution, insertions, microhomology, recurring deletions
				Total Chr1 from B6	134	15	
	B6 (b6/dba)	48	50	640000	2	1	insertions, microhomology, recurring deletions
	B6/DBA (b6/dba)	528	50	8800000	37	2	frequency, breakpoint distribution, microhomology, insertions, recurring deletions
	B6/DBA (b6)	144	50	2400000	12	1	insertions, microhomology, recurring deletions
				Total Chr1	185	19	
Chr19	B6	8	10	266667	1	0	breakpoint distribution, microhomology, insertions, recurring deletions
		760	50	12666667	58[b]	8	frequency, breakpoint distribution, microhomology, insertions, recurring deletions
				Total Chr19	59[b]	8	

[a] For the Chr1 hotspot pair, two different primer sets were used as indicated.
[b] For one deletion event, one breakpoint could not be precisely mapped.

Table S3. Insertions derived from other hotspots.

Hotspot pair	Insert origin	Insert start	Insert end	SPO11 activity at insert origin		Insert length (bp)	Deletion length (bp)	Microhomology at insert breakpoints (left/right)
				Atm$^{-/-}$	*Atm*$^{+/+}$			
Chr1	Chr3	116341240	116341350	cluster	no	111	2343	CAC/none
	Chr6	116019448	116019796	hotspot	cluster	349	2341	CACT/A
	Chr6	83540780	83540885	hotspot	cluster	106	1967	AG/none
	Chr7	41695870	41695945	hotspot	hotspot	76	1596	GTA/none
	Chr8	87936133	87936219	hotspot	hotspot	87	1513	(GATT insertion)/none
	Chr9	56053260	56053364	cluster	no	105	1671	C/TG
	Chr12	91711551	91711567	hotspot	hotspot	17	3326	CAAAGTGTCTG/TCT
	ChrX	69476686	69476920	hotspot	hotspot	235	2108	AT/none
Chr1 B/D	Chr9	55392465	55392589	no	cluster	125	2399	C/A
Chr19	Chr16	35066202	35066440	hotspot	hotspot	239	2005	none/none
	Chr17	78359789	78359826	hotspot	hotspot	38	2307	CA/none
	Chr17	80408805	80408819	hotspot pair	hotspot pair	15	1995	T/CAT

Hotspot pair	Insert from the non-PAR ChrY	Insert start	Insert end	SPO11 activity at insert origin		Insert length (bp)	Deletion length (bp)	Microhomology at insert breakpoints (left/right)
				Atm$^{-/-}$	*Atm*$^{+/+}$			
Chr1	insert 1* (2 of 26 repeats)	28785715	28785921	hotspot	hotspot	207	2253	A/G
		58748224	58748430	cluster	hotspot			
		90475833	90476039	no	hotspot**			
	insert 2* (1 of 15 repeats)	90476619	90476713	no	hotspot**	95	1939	AAACA/G
	insert 3 (3 of 26 repeats)	5658645	5658703	hotspot	cluster	59	1500	none/none
		5944098	5944156	hotspot	cluster			

* Inserts 1 and 2 are part of the same repeat; both match 12 copies of the repeat.

** Same hotspot.

Chr19	Insert from Chr1	88533343	88533493	microsatelite repeat $(CTT)_{27}$	148	2643	ACTGAGCTATCT/CCTCCTCCT

Table S4. Insertions derived from the hotspot pair.

Hotspot pair	Hotspot left or right	Insert length (bp)	Deletion length (bp)	Distance between deletion and insertion breakpoints (bp)	Microhomology at insert breakpoints (left/right)
Chr1	left	709	2590	4	none/GAAGG
	left	22	2411	28	none/AGA
	right	343	2334	11	TCCAGGGCAGTGC/none
	right	356	2437	0	TCCAGGGCAGTG/none
	right	356	2437	0	TCCAGGGCAGTG/none
Chr1 B/D	left	493	2025	40	TTG/AAAG
	right	302	2465	56	TCCAGGGCAGT/ATTC
	right	216	2399	3	GT/T
Chr19	left	204	2591	0	none/C
	right	231		3	CTCTCTC/none
	left	130	1361	0	none/ATAGCT
	left	132	1949	0	none/TAGCT
	right	16	2063	44	GCTCT/A

Table S5. Frequency of microdeletions in individual amplicons.

Genotype	Amplicon	No. reads	No. reads with deletions (unique[a])	Frequency (adjusted[b])	P value[c] versus *Atm*$^{-/-}$ (adjusted[b])	P value[c] *Spo11*$^{-/-}$ (adjusted[b])
Atm$^{-/-}$	1	3611491	60 (36)	1.66×10^{-5}		
	2	3072566	65 (39)	2.12×10^{-5}		
	3	3714378	50 (43)	1.35×10^{-5}		
	4	3240515	41 (31)	1.27×10^{-5}		
	Total	13638950	216 (149)	1.58×10^{-5}		
Atm$^{+/-}$	1	3615027	9 (7)	0.25×10^{-5}	<0.0001	0.0161
	2	4036817	4 (4)	0.10×10^{-5}	<0.0001	0.0825
	3	5334246	17 (16)	0.32×10^{-5}	<0.0001	0.0592
	4	4704066	10 (10)	0.21×10^{-5}	<0.0001	0.2799
	Total	17690156	40 (37)	0.23×10^{-5}	<0.0001	0.4670
Atm$^{+/+}$	1	5099332	23 (8)	$0.45 (0.20) \times 10^{-5}$	<0.0001 (<0.0001)	0.0004 (0.0387)
	2	4402709	53 (12)	$1.20 (0.73) \times 10^{-5}$	0.002 (<0.0001)	<0.0001 (0.0104)
	3	3360847	6 (4)	0.18×10^{-5}	<0.0001	0.6158
	4	3253036	5 (4)	0.15×10^{-5}	<0.0001	0.1313
	Total	16115924	87 (28)	$0.54 (0.33) \times 10^{-5}$	<0.0001 (<0.0001)	<0.0001 (0.0173)
Spo11$^{-/-}$	1	3339211	1 (1)	0.03×10^{-5}	<0.0001	
	2	2915459	8 (7)	0.27×10^{-5}	<0.0001	
	3	4485773	6 (6)	0.13×10^{-5}	<0.0001	
	4	3568282	12 (9)	0.34×10^{-5}	<0.0001	
	Total	14308725	27 (23)	0.19×10^{-5}	<0.0001	

[a]Total unique deletions obtained in that amplicon; note that the same deletion can be obtained independently in the overlapping amplicon.
[b]Adjusted frequencies and P values take into account potential jackpot events, in which 14 reads were obtained for the same microdeletion in amplicon 1, and 22 for another microdeletion in amplicon 2. Because these microdeletions were not obtained or were obtained just once in other amplicons they are considered to have arisen from PCR overamplification.
[c]Chi-square test.